HISTORIC
ENVIRONMENT
SCOTLAND

3D SURVEYING TECHNOLOGIES AND APPLICATIONS: POINT CLOUDS AND BEYOND

Technical report

By

Dr. Frédéric Bosché, Dr. Alan Forster and Dr. Enrique Valero

Heriot-Watt University

Royal Academy of Engineering Centre of Excellence in Sustainable Building Design

CyberBuild Research Lab

Table of Contents

Executive Summary

This report concludes a research project funded by Historic Environment Scotland (HES), led by Heriot-Watt University (Cyberbuild Lab of the Royal Academy of Engineering (RAE) Centre of Excellence for Sustainable Building Design) and in collaboration with Cyberhawk Innovations Ltd and Cambridge University (Construction Information Technology (CIT) laboratory). The project consisted of two main parts:

I. **A comparison of various 3D reality capture technologies for the survey of stone masonry walls.** Five technologies were uniquely considered, including: two different Terrestrial Laser Scanners (TLSs), a pole-mounted single-camera photogrammetric (PG) system, a UAV-mounted single-camera PG system, and a pole-mounted stereo-camera PG system.

II. **An investigation of novel algorithms to automatically extract 'first order' information from the acquired survey data that will be of ultimate interest to surveyors.** Survey data acquisition was traditionally characterised as a slow phase of the overall survey process. But, reality capture technologies have progressed dramatically in the last decade and data can now be obtained relatively rapidly. Today, the data processing stage is the one synonymous with 'time' heavy operations. This can be viewed as a 'switch' in the barrier to effective and efficient survey from data capture to data processing. As a result this part of the project aimed to demonstrate how automatic data processing approaches could significantly alleviate such barriers enabling wider and more cost effective utilisation of novel surveying technologies. Results are particularly reported on the automated segmentation of the survey data to differentiate individual components of stone masonry walls (i.e. stones and mortar), and on showing how this information could increase survey rapidity, effectiveness and objectivity.

This investigation was conducted adopting as a case study the 10m high rampart rubble masonry wall facing the East garden of Craigmillar Castle. Craigmillar is characterised as a medieval castle in Edinburgh, and is a category 'A' listed building of notable historical and cultural significance. The selected area of wall was ideal for both parts of this study, and in particular the second part (data processing) due to its relative complexity and more specifically: the random nature of the stonework; variation in width and depth of mortar joint; planar and curved surfaces; stone soiling and associate colour and texture variation.

The comparison of the different 3D reality capture technologies considered the accuracy and completeness (presence of areas for which no data was acquired) of the acquired data, as well as the efficiency of the data acquisition and pre-processing stages. The results confirmed the overall superiority of TLS over PG systems in terms of accuracy; nonetheless, the far cheaper pole-mounted PG system performed remarkably well with results not too dissimilar to one of the TLS systems. The UAV system's performance was poorer, but this was identified to be most likely the result of an insufficient overlap between images, which was itself the result of the use of a lens with an overly large focal length and the acquisition of too few pictures. Focusing on completeness, however, the limitations of ground-based TLS was visible at the top of the rampart (~10m), at which point the stones would occlude the mortar joint areas. In contrast, the mobility of the UAV, and to a lesser extent the use of the pole, ensured that all parts of the wall were acquired with the same level of point density with PG systems. With regard to efficiency, all systems were found to be equivalent at

least for survey jobs of this size. Furthermore, data acquisition typically required similar amounts of time for pre-processing (cleaning, and merging scans or conducting the photogrammetric reconstructions). UAV-based data acquisition appeared somewhat slower than pole-based acquisition due to the frequent need to change the battery. Overall, for larger projects, TLS may perform better if ground access is sufficient; yet the pole-mounted system can be a reasonable, cheaper alternative, and the UAV may in other contexts be the only option. Unfortunately, the stereo-camera PG system produced comparatively poor results because the tested system used industrial cameras that acquired images with low quality. It was thus not possible to demonstrate the potential added value of stereo PG over single-camera PG. It is recommended to re-compare UAV-based single-camera PG against pole-based single-camera PG, this time using camera systems with similar settings and lenses. A higher-quality (most likely custom-made) stereo-camera PG system should also be considered, as such a system could deliver reconstruction in metric scales.

This report highlights the fact that the rapid improvements in 3D reality capture technologies is alleviating the barrier to efficient survey associated with the acquisition stage. But, this work also logically reveals that processing of the acquired data is now considered the greatest time restriction. This ‘switch’ from acquisition to processing will have meaningful implications for project organisation and costing as ‘field work’ times are reduced and office based processing increase. Furthermore, this ‘switch’ means that renewed efforts need to be made in alleviating the barriers to efficient data processing.

Traditionally, limited research has been reported on the development of algorithms that can support surveyors in the processing of the vast amount of data associated with particularly complex tasks such as surveying random rubble masonry. These walling technologies have been particularly difficult due to the stones being variable in size and shape, not following uniform coursing and bonding, and the walls themselves not being necessarily planar. Within this context, novel analytical techniques could be developed that support the evaluation of movement of the wall or of specific individual stones, recessed mortar joints requiring repointing, etc. This report presents unique results that demonstrate that algorithms can be developed that can contribute in easing the data processing restrictions. It must be emphasised that these results are preliminary and further studies should be conducted to attain a more authoritative understanding of the capability and limitations of the technologies. Other applications should also be investigated. For example, it would be of interest to assess whether TLS or PG, along with well-crafted algorithms, could deliver accurate geometries of dimensional stones as required in cutting schedules.

The authors of this research and report, namely Dr. Frédéric Bosché, Dr. Alan Forster and Dr Enrique Valero (Heriot-Watt University), would like to thank Historic Environment Scotland, and especially Dr. Lyn Wilson and Dr. Alick Leslie, for funding this project, and also Mr. Robbie Nuttal and Mr. James Hepher for their support for the data acquisition at Craigmillar Castle. We would also like to thank Cyberhawk Innovations Ltd., in particular Mr. Stuart Thomas, for their support and UAV-based survey which were donated ‘in-kind’ to this project. Finally, we would like to thank Dr. Ioannis Brilakis and Mr. Carlo Minciacchi from the University of Cambridge for contributing to this project via the operation of their prototype stereo-camera PG system.

Authors

Dr. Frédéric Bosché is Associate Professor in the School of Energy, Geoscience, Infrastructure and Society at Heriot-Watt University, and leads the CyberBuild Laboratory that is part of the Royal Academic of Engineering Centre of Excellence in Sustainable Urban Design. Dr. Bosché's research focuses on the application of novel technologies in the Architectural, Engineering and Construction (AEC) sector, with specific contributions in reality capture, the processing of reality capture data, Building Information Modelling (BIM), and data visualization including with the use of novel immersive Virtual Reality (VR) and Augmented Reality (AR) systems. He has more than 50 publications, principally in international, peer-reviewed journals and conferences. In addition, he has received (PI) research grants from the Swiss National Foundation, InnovateUK, the UK Construction Industry Training Board (CITB), the British Council, and Historic Scotland. He is Associate Editor of the International Journal of Automation in Construction (Elsevier), and sits on the Board of Directors of the International Association of Automation and Robotics in Construction (IAARC). He received two best conference paper awards and several 'outstanding reviewer' awards for the quality of his peer reviews; and has delivered numerous invited presentations to both academic and professional audiences.

Dr. Alan Forster is Associate Professor in the School of Energy, Geoscience, Infrastructure and Society at Heriot-Watt University. He is the programme leader for MSc in Building Conservation (Technology & Management) and has 10 years industrial experience in Building Surveying, general construction and building conservation practice. His research is undertaken within the Royal Academic of Engineering Centre of Excellence in Sustainable Urban Design and focuses on: investigating traditional and low carbon building materials and construction technologies; building pathology and deterioration; building resilience to climate change; 'green' maintenance and building conservation philosophy, survey recording, evaluation and interpretation. Dr. Forster has around 50 published works, principally in international, peer-reviewed journals and conferences. In addition, he has attained (PI) research grants from: Engineering & Physical Sciences Research Council (EPSRC), Technology Strategy Board (TSB), Royal Society of Edinburgh (RSE), and the British Council. He was awarded a Senior Visiting Research Fellowship at the University of Bath in 2011, and the Royal Society of Edinburgh Bilateral exchange programme visiting Research Fellowship in 2014, at the Academy of Sciences for the Czech Republic. Professionally, he is a Fellow of the Chartered Institute of Builders (FCIOB); a Fellow of the Chartered Association of Building Engineers (FCABE); and an elected member of the Royal Institution of Chartered Surveyors (RICS) Building Surveying Professional group (Scotland). He is member of the Editorial Advisory Group for the RICS Building Conservation Journal, and for Structural Survey: Journal of Building Pathology & Refurbishment. He was awarded the 2010 Graduates Teaching Prize for lecturer of the year and the 2010 'Spirit of Heriot-Watt University' award for Pursing Excellence.

Dr. Enrique Valero is Research Associate in the School of Energy, Geoscience, Infrastructure and Society at Heriot-Watt University. His research focuses on reality capture and data processing, 3D object modelling and representation, and RFID technology. He received an MSc degree in Industrial Engineering, majoring in Mechanics, from the Universidad de Castilla-La Mancha, Spain, in 2008. He was awarded a Research Training Fellowship from the Spanish Ministry of Research, Development and Innovation in 2009. In 2013, he received a PhD in Computer Science from the Universidad Nacional de Educación a Distancia, Spain. After carrying out different research projects at Carnegie Mellon University (USA) and Katholieke Universiteit Leuven (Belgium), he joined the Cyberbuild Laboratory of the Royal Academic of Engineering Centre of Excellence in Sustainable Urban Design at Heriot Watt University, Edinburgh, UK. He has more than 20 publications, principally in international, peer-reviewed journals and conferences, and has already received two best conference paper awards for the quality of his research.

1 Introduction

The maintenance of the external fabric of buildings constitutes a large portion of overall building life cycle costs. Deterioration of external fabric is clearly exacerbated by the severity of environmental climatic conditions that act as 'agencies of materials change' causing accelerated weathering. The requirements of maintenance include both inspection and repair costs. Inspection systems and, more specifically, provision of access are an important cost of reactive and proactive (planned) maintenance intervention. It has been estimated that 10-20% of maintenance costs are associated with the provision of access for inspection; but, it is not unrealistic that complex scaffold solutions count for up to 40% of the total project cost. Alarmingly, almost 1/2 of construction fatalities and 1/3 of major injuries result from falls from height [1], many of which are associated with scaffolding. Clearly, cheaper and safer methods for accurate and complete inspection of building fabric would contribute to a significant reduction in maintenance and repair schedules and costs.

This situation is reflected in all types of construction, but is particularly important for historic buildings. This is due to the relative age and complexity of the fabric and associated degradation of the materials that may be many centuries old. Compounding this, the complexity of scaffold solutions (e.g. buttress and spire) can also be significantly greater than for newer structures that have considerations for access designed into them from 'first principles'. These solutions are clearly costly (sometimes up to 40% of total maintenance costs) and create higher levels of erection risk.

Compounding this situation, traditional reporting from building fabric inspection has been shown to be to greater or lesser degrees variable and therefore an objective starting point is not necessarily achieved. Straub [2] highlights this situation stating "*the practice of condition assessment by building inspectors yields variable results due to subjective perceptions of inspectors. Surveyor variability is defined as the situation where two or more surveyors, surveying the same building, arrive at very different survey decisions. This variability is caused by a variety of factors such as previous experience, attitude to risk and, heuristics – the use of 'rules of thumb' – a leaning towards a particular opinion regardless of the available evidence*." This may in turn hinder the determination of suitable repair requirements [3].

This project aimed to investigate how advanced reality capture and data processing technology can provide surveyors with objective, informative data pertaining to building fabric, in a rapid, safe and cost-effective manner. The information produced should support surveyors in ensuring objectivity, and thereby consistency, when assessing condition and suggesting repair strategies. The work summarised in this report consisted in the following two main parts:

I. **A comparison of various 3D reality capture technologies for the survey of stone masonry walls.** Five technologies were uniquely considered: two different Terrestrial Laser Scanners (TLSs), a pole-mounted single-camera photogrammetric (PG) system, a UAV-mounted single-camera photogrammetric system, and a pole-mounted stereo-camera photogrammetric system. The comparison of the technologies considered the accuracy and completeness (presence of areas for which no data was acquired) of the acquired data, as well as the efficiency of the data acquisition and pre-processing stages.

II. **An investigation of novel algorithms to automatically extract 'first order' information from the acquired survey data that will be of ultimate interest to surveyors.** Survey data acquisition was traditionally characterised as a slow phase of the overall survey process. But, reality capture technologies have progressed dramatically in the last decade and data can now be obtained relatively rapidly. Today, the data processing stage is the one synonymous with 'time' heavy operations. As a result, this part of the project aimed to demonstrate how automatic data processing approaches could significantly alleviate such barriers enabling wider and more cost effective utilisation of novel surveying technologies. Results are particularly reported on the automated segmentation of the survey data to differentiate individual components of stone masonry walls (i.e. stones and mortar), and on showing how this information could increase survey rapidity, effectiveness and objectivity.

This report is organised as follows. Section 2 first provides a concise review of previous research on assessing novel 3D reality capture technologies for surveying historic buildings; these essentially include TLS and PG. The section also reviews recent developments in information and communication technologies (ICTs), including Building Information Modelling (BIM), to support the management of surveyed data and inferred information for the maintenance of the fabric of historic monuments. The literature concludes with the identification of the need for new algorithms to process reality capture data to extract the information of actual value to surveyors. Section 3 then presents the experiment conducted to compare the five 3D survey technologies mentioned above. The results demonstrate the strengths of modern laser scanners in terms of data precision but also confirm their limitation in terms of access. PG systems appear generally inferior (although not always significantly) but offer great potential in terms of access, efficiency and cost. Section 4 demonstrates the feasibility and value of using automated data processing algorithms, by reporting results obtained with a novel data processing system that automatically processes 3D point clouds of stone masonry walls. The system first segments the wall into the individual stones and mortar regions, and then reports valuable information about the length of mortar joints, their depth (and thus whether there are recessed zones) and where pinning should be considered during repair and maintenance. This information would help surveyors in objectively assessing and accurately quantifying repair needs in a targeted manner. Section 5 concludes the report with recommendations for the implementation of the investigated technologies in practice as well as for future research.

2 Background

In 1995, Ogleby [4] reviewed the advances made in the techniques and technologies for creating records of significant sites and monuments. He especially focused on photogrammetry, and remarked the growing interest in "digital image processing". Being only 20 years old, Ogleby's paper constitutes a good reference to understand the significant progress that has been made since in: reality capture technologies to acquire data; and Information and Communication Technologies (ICTs) to manipulate, organize and visualize the acquired data. This section will successively review modern reality capture technologies, with focus on 3D imaging technologies, and then ICTs that are being considered for data processing (i.e. information extraction) and information management.

2.1 Laser Scanning

Laser scanning is a very recent technology (it was unknown to Ogleby in 1995) but constitutes a revolution to land and monument surveying. Modern laser scanners sweep their surrounding space with a laser beam to obtain dense and accurate point clouds. While laser scanners can be used airborne mounted on planes or helicopters to capture land elevation (in this case experts refer to the technology as *LiDAR*), in the context of monument recording it is more commonly used ground-based, in which case it is best referred to as *Terrestrial Laser Scanning (TLS)*.

Within the context of historic monument survey, noteworthy examples of the use of TLS include the work of Wilson et al. [5] who illustrate the distinct benefits of TLS for the survey of large and complex historic monuments via case studies of UNESCO World Heritage Sites, including New Lanark in Scotland, Rani ki Vav stepwell in India and the Sydney Opera House in Australia. Cardaci et al. [6] show that TLS provides significant value compared to traditional manual survey. They also show how CAD models generated from the data can be successfully used for structural analysis using the Finite Element Method (FEM). Nettley et al. [7] use TLS and LiDAR to obtain a photorealistic geospatial model of the historic quayside at Cotehele Quay, integrated in an accurate Digital Elevation Map (DEM) in order to assess the potential impact of rising sea levels resulting from climate change. Temizer et al. [8] show the value of TLS to survey underground structures like the Byzantine cistern situated beneath the court of the Sarnicli Han building. They also investigate the impact of various levels of point filtering on the accuracy of the mesh produced from the data. De Matias et al. [9] investigate the use of TLS for surveying historic structures like walls, pillars and vaults. In particular, using the Coria Cathedral as a case study, they show how it can be used to measure structural displacements (e.g. wall collapse) and link those to cracks manually extracted from the data.

2.2 Photogrammetry

As the review of Ogleby [4] shows, photogrammetry (PG) is actually a well-established method for obtaining 3D records of historic monuments. Nonetheless, significant progress has been made in the last two decades, both in terms of hardware and software, to rapidly and accurately obtain the records. Most importantly, high-resolution and portable digital cameras are now widely available at a relatively low cost. Furthermore, the development of robust automated feature detection and matching in digital images, (e.g. SIFT [10] or SURF [11] features), as well as dense matching approaches [12] have dramatically improved the image processing stage, enabling entirely automated processing pipelines. Thanks to the small weight of modern cameras, single-camera photogrammetry has shown great potential to resolve access-related issues while producing good-quality dense textured 3D point clouds and meshes.

Within the context of historic monument survey, noteworthy examples of the use of PG include the work of Cappellini et al. [13] who apply PG to produce 3D models of monuments that are used to generate 2.5D orthophotos of walls. Using the example of Roman walls, these orthophotos are used to conduct the semantic annotation of the *opus* of different sections of the wall.

The main limitation of PG systems is however that they are not robust to varying lighting conditions and texture-poor or reflective materials. Furthermore, their accuracy quickly drops in comparison of that of laser scanners. Finally, single-camera PG systems provide 3D reconstructions only up to scale, and require the user to extract known dimensions in the scene to adequately scale the reconstructions.

The wide majority of prior works, such as those above, consider single-camera PG systems due to their simplicity of deployment. Yet, stereo-camera photogrammetric systems could also be considered as they have the advantage of providing data in metric scale – the scaling process takes advantage of the known/calibrated distance between the two cameras (called *baseline*) and their relative orientation (*vergence*). Furthermore, stereo-camera PG systems can theoretically provide more precise reconstructions – due to the availability of more data and pre-calibrated pairs of images. However, these systems have not been widely studied in the building environment in general, and the historic building environment in particular. That said, noteworthy examples include the recent works of Brilakis et al. [14] as well as that of Bruno et al. [15], the latter focusing on underwater artefact 3D reconstruction.

2.2.1 Aerial Photogrammetry

Photogrammetric reconstructions need perpendicular and oblique images taken from strategic points to obtain a good resolution and accurate modelling. A pole-based system can be considered to take pictures higher than human height. However, poles can only be comfortably used up to approximately 5m heights, and aerial solutions must be considered above this.

Aerial photogrammetry has long been conducted using planes or helicopters with under-mounted camera systems (similarly to LiDAR systems). Yet, recent and rapid developments of Unmanned Aerial Vehicles (UAVs) are providing a new platform for photogrammetric system that further resolve access issues.

The value of UAVs to surveying has already been demonstrated in various context such as for ecological surveys [16, 17] or structural surveys [18, 19]. All these works show how avoiding the use of planes or scaffolding systems is beneficial to reduce acquisition time and budget.

In the context of historic monuments, UAV-based photogrammetry has been studied to provide alternative solutions to TLS. For example, Puschel et al. [20] propose the use of terrestrial and UAV pictures to create an accurate 3D model of Castle Landenberg, using tie points as a reference to accurately model the building. Remondino et al. [21] review the different stages of data acquisition and processing, such as: planning, camera calibration, 3D reconstruction and applications. Remondino [22] provides an extensive review of devices and software for recording and modelling oriented to Cultural Heritage (CH). Lately, Koutsoudis et al. [23] proposed a photogrammetric system combining UAV and terrestrial pictures and compared the resulting reconstruction with TLS, obtaining promising results. In constrast, Xu et al. [24] actually combine 3D data from TLS and a UAV-mounted camera for the reconstruction of a historical monument in Fujian, China. TLS point clouds are used to model the façades and photogrammetric information is used to complete the roof area.

2.3 Data Processing and Management

2.3.1 HBIM

The Architectural, Engineering, Construction and Facilities Management (AEC/FM) sectors are experiencing the rapid development of Building Information Modelling (BIM) as a means to more efficiently and effectively build, operate and maintain building assets [25]. This management (r)evolution also applies to historic monuments and could enable a more collaborative management of historic monuments with models that integrate all relevant data and information to enhance interpretation and visualization. In this context, experts use the term Historic BIM (HBIM) [26, 27].

At the core of a (H)BIM model is a parametric, semantically-rich 3D model. When a BIM model is to be generated for an existing model, the state of the art is to employ point clouds obtained by TLS [25, 28]. Hichri et al. [29] provide a general review of the stages to go from point cloud to BIM, also discussing pre-processing and data representation matters. Various other researchers have also proposed approaches to semi-automatically generate 3D models of historical buildings from point clouds. Macher et al. [27] divide the building in sub-spaces, model surfaces and fit primitive shapes to architectural elements. Oreni et al. [30] present a workflow using NURBS and vector profiles to model the geometry of historic monument components. And Garagnani and Manferdini [31] present a Revit plug-in (GreenSpider) that matches a spline to imported 3D points.

2.3.2 Semantic Labelling/Segmentation

The aforementioned works demonstrate the interest of heritage experts to use TLS and PG data to better record the state of historic monuments, and even generate and maintain life-cycle 3D (H)BIM models of them. However, it is important to realize that TLS or PG point clouds (or generated meshes) are just 'raw' data, and the *information* truly valuable to experts needs to be extracted from that data, through its segmentation and semantic labelling. This is particularly important to the study of material and structural defects. This subsection is devoted to review works related to the study of TLS and PG data to detect, segment and label material or structural defects.

Current practice to the evaluation of masonry defects, whether using TLS/PG data or more traditional surveying methods, is based on visual observations, and subsequently manual data segmentation and labelling. For example, numerous authors show how ortho-photos obtained from 3D reality capture data can be used for manual labelling and mapping of degradation, e.g. using the ICOMOS glossary [32, 33, 34, 35]. Photogrammetry appears particularly appropriate for this kind of analysis because of the typically higher quality of the images in terms of colour and texture, which is valuable to defect labelling.

Manual segmentation and labelling are however time-consuming and not necessarily very accurate and repeatable (i.e. they vary with surveyors and experience). Researchers have thus looked into developing (semi)-automated segmentation and labelling algorithms. For example, colour could be automatically processed to characterise materials and degradation in fabric. For example, Moltedo et al. [36] investigate compression, entropy and gradient analysis for characterising materials in images. Cossu et al. [37] similarly investigate histogram threshold and edge detection techniques to detect, segment and label stone degradation regions, characterized by holes or cavities, in colour images. Thornbusch [38] analysed colour images of road-side stone walls over a six-year period using basic image segmentation tools from Photoshop (e.g. histogram analysis) to semi-automatically detect soiling and decay, as well as their evolution over the period. However, they highlight that "*variation in external lighting conditions between re-surveys is a factor limiting the accuracy of change detection.*"

Other authors base their works on more complex data analysis techniques. In [39], Kapsalas et al. compare various segmentation algorithms, such as region-growing or difference-of-Gaussians to detect the topology and patterns of stone corrosion (black crust) in close-range 2D colour images. Cerimele and Cossu [40, 41] also apply region-growing algorithms to detect decay regions of sand stones (sediment or cavity decays) in 2D colour images, given seed pixels selected by the user. And finally, a semi-automatic delineation and masonry classification is carried out by Oses and Dornaika [42] who use Artificial Intelligence techniques (k-NN classifiers) to identify stone blocks in 2D images.

Most of these works focus on using 2D colour information to identify and evaluate defects. However, 3D data can also be valuable to such analysis. In fact, there is value in conducting segmentation and labelling by collectively using 3D and colour information. With this strategy, Cappellini et al. [13] propose a semi-automatic approach to semantically label 2.5D data (colour and depth profile) of walls obtained using photogrammetry. The authors focus on labelling the wall opus using image processing techniques and parametric models of the opus. The opus model parameters include the "*geometrical shape and dimensions of the stones or bricks, [and] the presence of the intervals amongst them and their installation*".

2.4 Summary

In summary, a large quantity of research focuses on assessing the suitability of Terrestrial Laser Scanning (TLS). While TLS presents great advantages in terms of data density and accuracy, its application to building fabric surveying is limited by the need to set up the scanner on the ground or a stable platform at multiple locations that altogether provide a complete 3D survey of the entire building fabric. TLS is thus not ideal for situations such as the assessment of mortar joints in high stone walls or the assessment of roofs. Single-camera photogrammetry (PG) has shown great potential to resolve access-related issues while producing good-quality dense textured 3D point clouds/meshes. Performance can however be significantly limited by the texture and/or type of material being scanned. Furthermore, 3D data provided by photogrammetric systems has unknown scale; control networks or known dimensions in the data are necessary to convert the data to metric scale, which introduces additional error. Stereo-camera PG has the advantage of providing data in metric scale and may be more robust that single-camera PG. However, these systems have not yet been considered for the survey of historic (and CH) monuments.

As a result of the prior research reported above, it was felt relevant to conduct a systematic comparison of various 3D surveying technologies including: two different terrestrial laser scanners (Faro Focus 3D and Leica ScanStation P40), a pole-mounted single-camera photogrammetric system, a UAV-mounted single-camera photogrammetric system, and a pole-mounted stereo-camera photogrammetric system. In particular, the study aimed to compare the two TLS systems, assess the performance of the single-camera photogrammetric systems against that of the TLS systems, and investigate whether a stereo-camera photogrammetry could indeed provide additional value over single-camera ones.

The literature review above indicates that greater effort has been invested into investigating the potential of TLS and PG for the survey of monument, and the overall conclusion is that they are both valuable but for different reasons, in different contexts. In fact, we argue that the barriers to the wide, systematic use of the technologies in practice is now less about their data acquisition performance, but increasingly the large amount of expert manpower that is required to extract the information of value from the acquired data. With the growing interest in (H)BIM, surveyors and other monument management experts need much more efficient methods to structure the 'raw' data provided by TLS and PG systems and extract from the data the valuable information they need. For example, by segmenting TLS data of the fabric of a building into the building fabric's sub-components (e.g. walls, windows, roof), then the progressive evaluation of buildings (deterioration) over time can be significantly improved both in quality and speed. Endeavouring to demonstrate this, this study presents results obtained with novel algorithms developed by the authors that offer such valuable functionality. These algorithms are developed with focus on stone masonry.

3 Comparison of 3D Survey Technologies

The first part of this study consisted in comparing various 3D survey technologies on the same test site with the same conditions. Sections 3.1 and 3.2 introduce the investigated survey technologies and the test site respectively. Section 3.3 presents the data acquisition campaign and the pre-processing necessary to generate the datasets employed in the comparison. Section 3.4 reports the results obtained when comparing the datasets delivered by the various technologies. Section 3.5 concludes this section with observations leading to the need to switch or widen R&D focus from the data acquisition stage to the data processing stage, i.e. extracting the information of value to surveyors from the acquired data.

3.1 3D Survey Technologies

The literature clearly shows that two main modern technologies are now considered by CH experts for obtaining 3D records of historic monuments: laser scanning and photogrammetry. This project aims to further compare these technologies with the goal to assess whether photogrammetry delivers sufficient quality to be considered a real alternative in practice. Indeed, while TLS presents great advantages in terms of data density and accuracy, its application to building fabric surveying is limited by the need to set up the scanner on either the ground or a stable platform at multiple locations that altogether provide a complete 3D survey of the entire building fabric. For example, ground-based laser scanning may not be suitable to investigate the deterioration of masonry and mortar joints on the upper parts of high stone walls. In contrast photogrammetric systems have the advantage of being cheaper and more portable (e.g. mounted on a UAV). So, if their performance is sufficient, then they could be considered a serious alternative to terrestrial laser scanning systems.

More specifically, this project aimed to compare the following survey systems, including two TLS systems and three PG systems:

- TLS 1 | Leica ScanStation P40
- TLS 2 | Faro Focus 3D
- PG 1 | Pole-Mounted Single-Camera Nikon D810
- PG 2 | UAV-Mounted Single-Camera Sony Alpha-7R
- PG 3 | Pole-Mounted Stereo-Camera Imaging Source DFK 23UP031

The five systems are introduced in the following sub-sections.

3.1.1.1 TLS 1 | Leica ScanStation P40

Among the different strategies used in the manufacturing of laser scanners, *time-of-flight (TOF)* [43] is the most important technology. The time-of-flight technology is mainly used for long range laser scanners, which can measure points hundreds of meters away from the scanner. These devices emit electromagnetic pulses that return to the TLS after colliding an object. The time elapsed in this operation is used to calculate the distance between the scanner and targets.

The Leica ScanStation P40 (Figure 1) is the latest TOF scanner produced by Leica, and is advertised as having very good performance, as summarized in Table 1. We particularly note that the scanner should be able to scan objects up to 270m away, with an accuracy of ±3mm at 50m.

Figure 1: Leica ScanStation P40.

Table 1: Performance characteristics of the Leica ScanStation P40.

Range	From 0.4m to 270m
Scan rate	Up to 1,000,000 points per second
Wavelength	1550nm
Laser Class	1
Single-point precision	±3mm at 50m; ±6mm at 100m
Field of view	360° horizontal; 270° vertical

3.1.1.2 TLS 2 | Faro Focus 3D

A variation of the TOF technology is the *phase-based* method [43]. In this case, a continuous wave is emitted by the scanner. After reaching the objective, the signal returns to the scanner and the phases of the emitted and received waves are compared to calculate the distance between the scanner and the measured object. A limitation of *phased-based* technology, however, is that it is limited to shorter ranges.

The Faro Focus 3D (Figure 2) is a recent phase-based scanner by Faro. Its performance characteristics, summarized in Table 2, show that this scanner can measure distances up to 120 meters (although in practice, it is often recommended not to exceed 80m), with slightly lower but still good single point precision. An additional important advantage of the Faro Focus 3D scanner is that it is significantly smaller than scanners such as the Leica ScanStation P40, which makes it more portable (for transportation).

Figure 2: Faro Focus 3D.

Table 2: Performance characteristics of the Faro Focus 3D.

Range	From 0.6m to 120m
Scan rate	Up to 976,000 points per second
Wavelength	905nm
Laser class	3R
Single-point precision	±2mm at 25m
Field of view	360° horizontal; 300° vertical

3.1.1.3 PG 1 | Pole-Mounted Single-Camera Nikon D810

The first single-camera photogrammetric system considered is a digital single-lens reflex (DSLR) camera Nikon D810 equipped with a 14mm lens that is mounted on an extendable pole and operated manually (Figure 3). This camera can obtain 36 megapixels pictures and the system allows the surveyor the acquisition of high-quality data at heights up to 5 meters. The weight of the camera and lens together is 1,550g (880g + 670g respectively). This adds up to 4kg when adding the carbon-fibre pole.

The characteristics and settings of the camera for this acquisition campaign are summarized in Table 3.

Figure 3: Surveyor operating the pole-mounted Nikon D810 camera.

Table 3: Characteristics and setting of the Nikon D810 camera employed for this acquisition campaign.

Resolution	36.3MPx
Sensor	35.9 x 24mm
ISO sensitivity range	64 to 12,800
Focal length	14mm
Weight (camera and lens)	1.5kg

3.1.1.4 PG 2 | UAV-Mounted Single-Camera Sony Alpha-7R

A pole-based system can be used to take pictures up to the pole height (typically 5m). Also, users have to carry a relatively heavy load associated with equipment dead load during the data acquisition process. Therefore, the second single-camera photogrammetric system considered is a digital single-lens reflex (DSLR) camera Sony Alpha-7R equipped with a 35 mm lens that is mounted on a UAV and operated remotely. This camera can obtain 36 megapixels pictures. The total weight of the camera and lens is 627 g (407g + 120g). The characteristics and settings of the camera for this acquisition campaign are summarized in Table 4. The UAV employed here (note that this is the standard system employed by our partner, Cyberhawk Innovations, at the time of the study) is an Asctec Falcon 8 Multi-rotor with characteristics summarised in Table 5.

Note that the verticality of the rampart, the proximity to the façade and the potential for GPS multipath prevented a normal autonomous flight planning. As a result, the pilot had to command the UAV and trigger the camera manually.


Figure 4: Left: A view of the UAV-mounted single-camera Sony Alpha-7R system during data acquisition. Right: Close-view of the UAV system.

Table 4: Characteristics and setting of the Sony Alpha-7R camera employed for this acquisition campaign.

Resolution	36.8MPx
Sensor	35.9 x 24mm
ISO sensitivity range	50 to 25,600
Focal length	35mm
Weight (camera and lens)	0.63kg

Table 5: Characteristics of the UAV employed with the Sony Alpha-7R camera for this acquisition campaign.

Payload	Sony Alpha 7R DSLR and 35 mm prime lens
Maximum permitted flying height	120m (Civil Aviation Authority regulations)
Flight time	Up to 12 minutes
Aerial scheme	Vertical lines from left to right
Overlap between pictures	75% (estimated)
Shots frequency	Manually triggered to achieve required overlap

3.1.1.5 PG 3 | Pole-Mounted Stereo-Camera System

Finally, a stereo vision-based photogrammetric system is considered. The system used in this experiment is a prototype (see Figure 5) conceived by researchers of the Construction Information Technology (CIT) laboratory at the University of Cambridge. This system consists of two industrial cameras DFK 23UP031 by Imaging Source and equipped with 8mm lenses. Both cameras and their wiring are enclosed in an aluminium chassis. Left and right cameras produce 5 megapixel pictures and have parallel epipolar lines and a distance between them (baseline) calibrated to 38cm. The system delivers pairs of 5 megapixels pictures, and can be mounted on a pole like other camera systems. The weight of the system without the pole is 1.24kg (2x65g for the cameras, 2x156g for the lenses, 0.8 kg the housing). The characteristics and settings of the stereo system for this acquisition campaign are summarized in Table 6.

Figure 5: Stereo Vision-based Photogrammetric System.

Table 6: Characteristics and setting of the Imaging Source DFK 23UP031 cameras employed for this acquisition campaign.

Resolution	5MPx
Sensor	5.7 x 4.28mm
ISO sensitivity range	N/A
Focal length	8mm
Weight (system)	1.24kg

3.2 Test Site: Craigmillar Castle

A large stone wall of the rampart of Craigmillar Castle in Edinburgh (Figure 6) has been selected as test site. The castle was built by the Preston family in the 14th century and is currently managed and maintained by Historic Environment Scotland. It is a good example of medieval castellated architecture and is culturally significant.

Figure 6: Craigmillar Castle.

Five locations inside the castle were considered and evaluated for the test site. Exterior and interior random rubble walls were thoroughly examined, considering their advantages and disadvantages (shown in Figure 7). Several parameters, listed in Table 7, were evaluated:

- *Sufficient height*: to study the performance of the chosen technologies at increasing heights;
- *Wind protection*: especially for the UAV as collision with the monument must be avoided and the acquisition of pictures with good quality requires the UAV to be in sufficiently stable positions;
- *Accessibility*: There should not be trees or other occlusions preventing the safe use of the UAV and occluding the acquisition of data for all systems.
- *Curved wall sections*: Presence of curved wall sections is of interest to demonstrate the robustness of any algorithm to evaluate non-planar walls (many existing algorithms assume planar walls).

The evaluation was conducted in collaboration with Historic Environment Scotland and Cyberhawk Innovations Ltd. survey experts, and led to the selection of the wall Section 2 (see Figure 7).

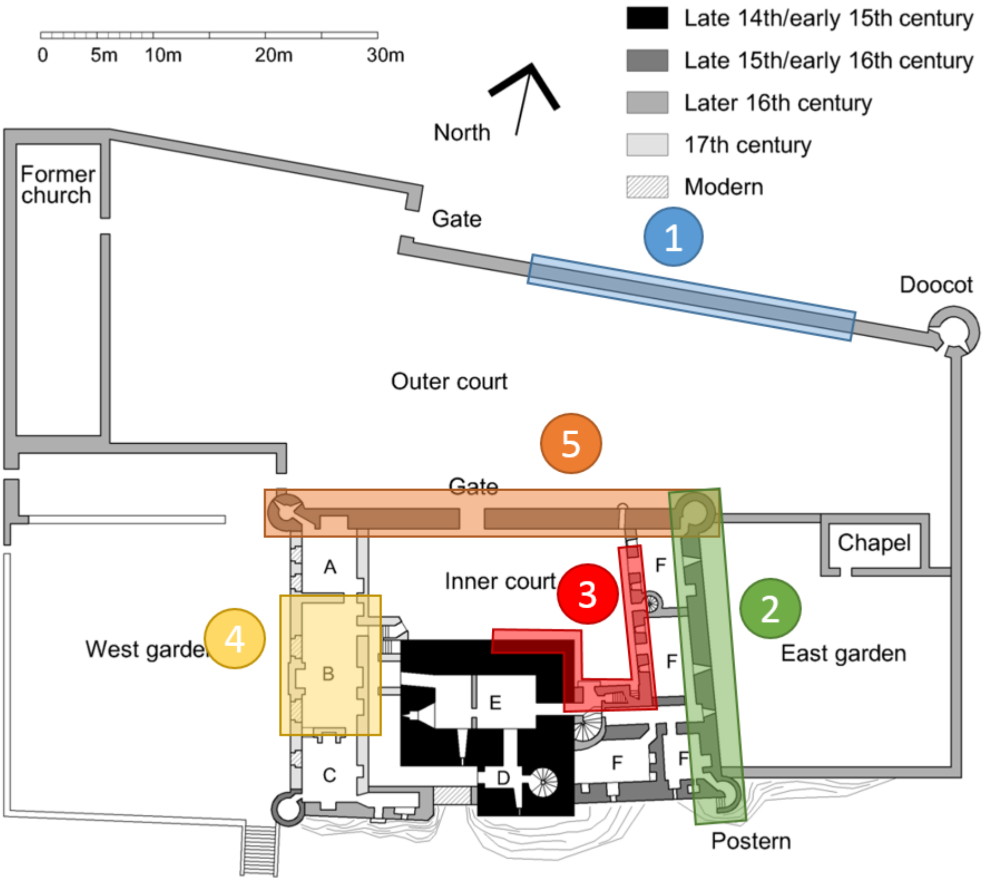

Figure 7: Survey sites considered for the experiment.

Table 7: Site selection criteria.

Site selection criterion	Site 1	2	3	4	5
Sufficient height	-	✓	✓	✓	✓
Wind protection	-	✓	✓	✓	-
Curved walls	-	✓	-	-	✓
Accessibility	✓	✓	-	-	✓

3.3 Data Acquisition and Pre-Processing

The above-mentioned photogrammetric and laser scanning systems were all transported to site on Wednesday 13th May 2015 with all data acquisition occurring on that day. Data acquisition was preceded by the establishment of a geo-referenced survey network that was used to (1) align all datasets within the same (geo-referenced) coordinate system, and (2) scale the 3D data coming from the photogrammetric systems. These steps, along with the pre-processing of the acquired data are detailed in the following.

3.3.1 Survey Network

A survey network composed of three geo-referenced tie points set with 6-inch circular targets was established within the East garden site for geo-referencing the TLS data. This network was geo-referenced using additional tie points set at pre-established geo-markers. All measurements for the establishment of the network were conducted using a Leica MS50 multistation. Figure 8 shows a picture of one of the tie points and Figure 9 shows a top view of the garden with the location of three tie points.

Figure 8: One of the three tie points set up with a 6-inch circular target.

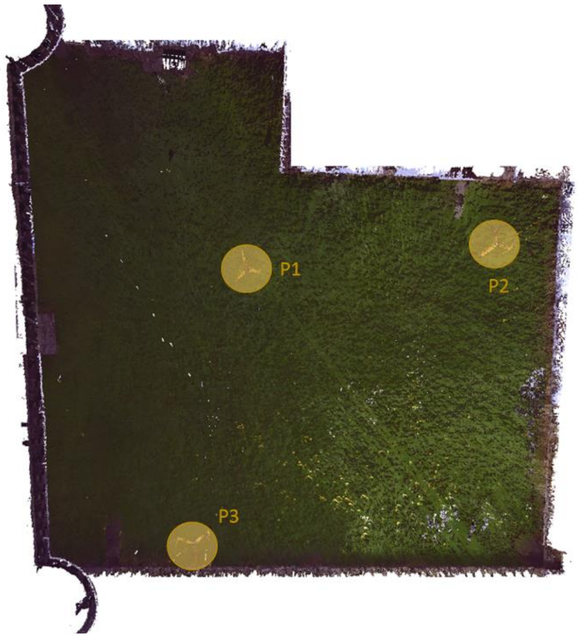

Figure 9: The survey control network for the two TLS devices.

While the above survey network can be used to geo-reference the TLS point clouds, the targets of those tie points cannot be properly digitised during the data acquisition process with PG systems. This is due to the impossibility to simultaneously focus the camera on the wall and the tie point target. Therefore, a second survey network had to be established with a different set of targets (17cm checkerboard targets) fixed to the walls and geo-referenced by means of the MS50 multistation. Figure 10 shows a picture of one of the tie points and Figure 11 shows a perspective view of the garden with the location of the tie points.

Figure 10: One of the squared targets attached to the walls.

Figure 11: The survey control network for the PG systems.

3.3.2 TLS 1 | Leica ScanStation P40

To ensure a full coverage of the garden, three laser scans were acquired with the Leica ScanStation P40 laser scanner (see Figure 12). The three scans were then aligned using the survey network, resulting in a unified clean point cloud containing 374 million points. An orthophoto of the point cloud corresponding to the castle rampart wall facing the garden is provided in Figure 13; that section of the point cloud alone contains 180 million points.

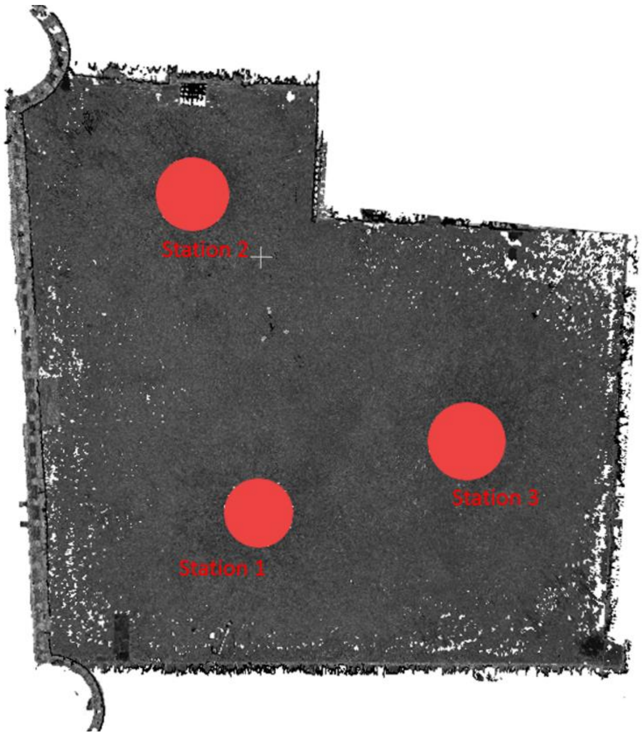

Figure 12: Leica ScanStation P40 locations for data acquisition.

The registration of the three scans into a unified and geo-referenced point cloud was achieved by automatically finding and matching the tie points in the three scans to the corresponding tie points in the survey network. Given these matches, an optimal (but never perfect) alignment was calculated. This optimisation residual error (i.e. *registration residual error*) can be presented in two parts: the *scan alignment residual error* that assesses the alignment between scans, and the *geo-referencing residual error* that assesses the geo-referencing error. Summarized in Table 8, the geo-referencing residual errors for all tie points for all scans (i.e. all stations) are all under 2mm. Summarised in Table 9, the alignment residual errors for all tie points in any pair of scans never exceed 1mm.

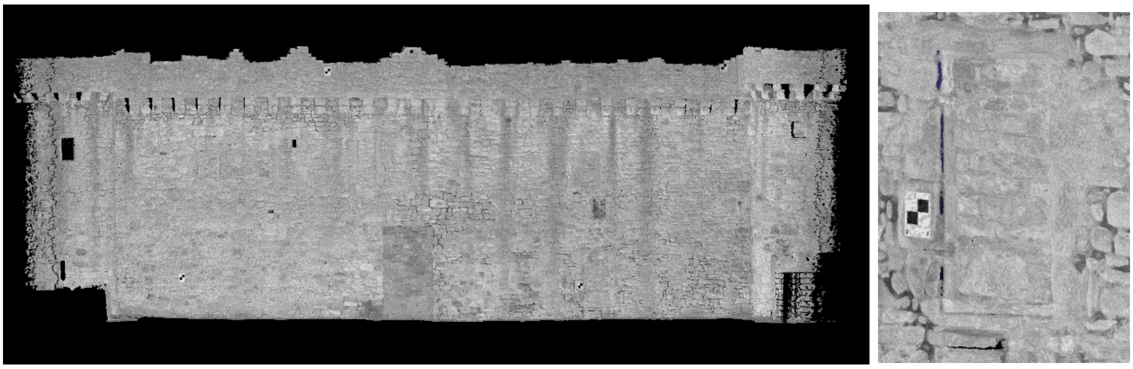

Figure 13: Point cloud of the rampart wall facing the East garden obtained by the Leica TLS; Right: detail of a blocked-up window. The point cloud is coloured based on the signal reflectivity recorded by the scanner.

Table 8: Residual errors for the geo-referencing of the Leica ScanStation P40 data.

Tie point Constraint	Data Source	Data Source	Error [mm]
P1	Total Station	Station 1	2
	Total Station	Station 2	2
	Total Station	Station 3	2
Mean			**2**
P2	Total Station	Station 1	1
	Total Station	Station 2	1
	Total Station	Station 3	1
Mean			**1**
P3	Total Station	Station 1	2
	Total Station	Station 2	1
	Total Station	Station 3	2
Mean			**1.6**

Table 9: Residual errors for the alignment of the three Leica ScanStation P40 scans into a unified point cloud.

Tie point Constraint	Data Source	Data Source	Error [mm]
P1	Station 1	Station 2	1
	Station 1	Station 3	1
	Station 2	Station 3	1
Mean			**1**
P2	Station 1	Station 2	1
	Station 1	Station 3	1
	Station 2	Station 3	0
Mean			**0.6**
P3	Station 1	Station 2	1
	Station 1	Station 3	1
	Station 2	Station 3	1
Mean			**1**

3.3.3 TLS 2 | Faro Focus 3D

The same procedure was applied for the data acquisition using the Faro Focus 3D, with three scans acquired at similar locations, as shown in Figure 14. The final unified point cloud contains 87 million points overall, and 51 million points for the rampart wall section alone. In this case, colour information has also been acquired using the Faro Focus 3D internal camera. The point clouds shown in Figure 14 and Figure 15 are coloured using that acquired colour information.

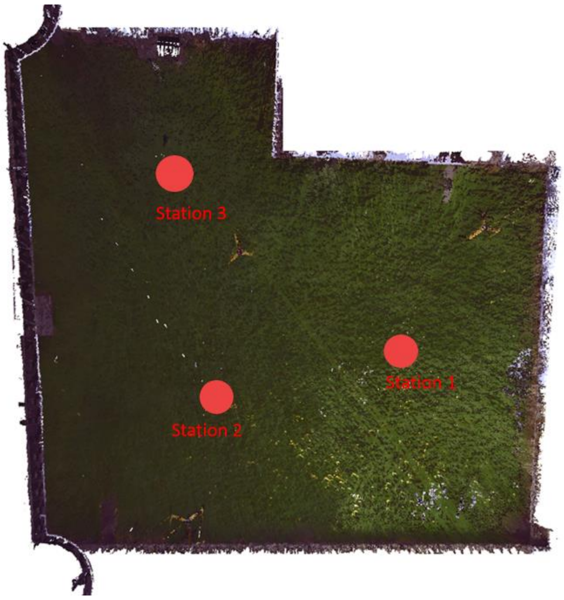

Figure 14: Faro Focus locations for data acquisition.

Figure 15: Point cloud of the rampart wall facing the East garden obtained by the Faro Focus 3D TLS. Right: detail of a blocked-up window. The point cloud is coloured with the true colour acquired by the scanner.

The registration residual error is studied in the same way as for the TLS 1 system. Summarized in Table 10, the geo-referencing residual errors for all tie points for all scans are between 2mm and 8mm. Summarised in Table 11, the alignment residual errors for all tie points in any pair of scans are between 2 and 7mm.

Table 10: Residual errors for the geo-referencing of the Faro Focus data.

Tie point Constraint	Data Source	Data Source	Error [mm]
P1	Total Station	Station 1	8.1
	Total Station	Station 2	3.4
	Total Station	Station 3	2.3
Mean			**4.6**
P2	Total Station	Station 1	3.9
	Total Station	Station 2	2.8
	Total Station	Station 3	1.6
Mean			**2.8**
P3	Total Station	Station 1	7.3
	Total Station	Station 2	2.5
	Total Station	Station 3	1.5
Mean			**3.8**

Table 11: Residual errors of the alignment of the three Faro Focus scans into a unified point cloud.

Tie point Constraint	Data Source	Data Source	Error [mm]
P1	Station 1	Station 2	5.8
	Station 1	Station 3	6.7
	Station 2	Station 3	1.1
Mean			**4.5**
P2	Station 1	Station 2	1.6
	Station 1	Station 3	3.1
	Station 2	Station 3	2.2
Mean			**2.3**
P3	Station 1	Station 2	6.5
	Station 1	Station 3	5.9
	Station 2	Station 3	1.8
Mean			**4.7**

3.3.4 PG 1 | Pole-Mounted Nikon D810

Aiming to generate a 3D point cloud of the garden through a photogrammetric process, 260 pictures were taken from many locations around the garden and with different orientation. The distance of the camera to the walls was kept to 4-5 metres, with a few additional pictures taken at further distances. Figure 16 shows the position and orientation of the camera for all the pictures acquired and used for the photogrammetric reconstruction using the PG 1 system. While some of the images were acquired at human height by hand, other images (specifically for the rampart wall) were acquired with the camera mounted on the pole (and triggered using a mobile phone app) that could extend up to 5m.

The photogrammetric reconstruction using the 260 images was conducted using Agisoft PhotoScan v.1.1.6, delivering a dense point cloud containing 79 million points overall, including 51 million points for the rampart wall section. Figure 17 shows the rampart wall point cloud. It is interesting to note that the colours are brighter and generally appear more realistic than those obtained using the Faro scanner (see Figure 15).

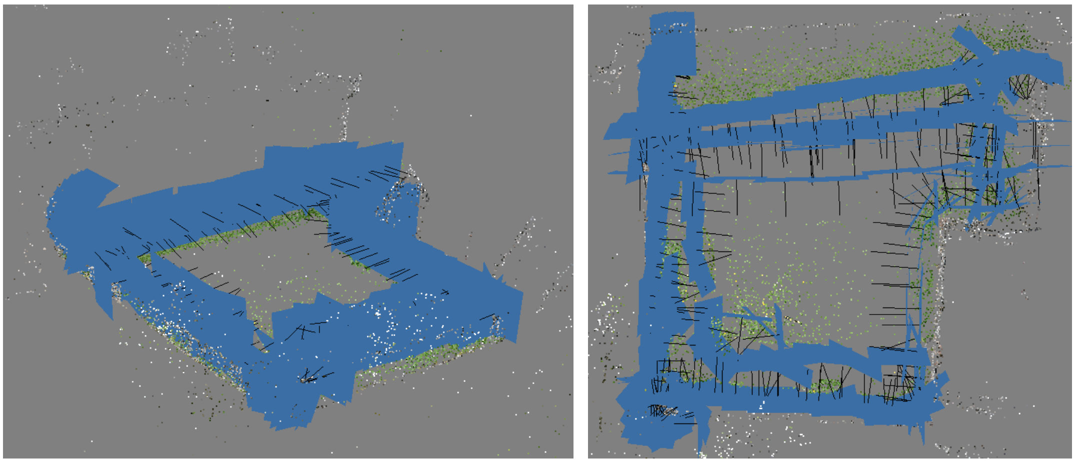

Figure 16: Camera positions and camera planes for the acquisition using the pole-mounted Nikon camera. Left: Perspective view; Right: top view. Each position is represented by a dark line and blue rectangle that represent the camera frustrum.

Figure 17: Point cloud of the rampart wall facing the East garden obtained by the pole-mounted Nikon camera. Right: detail of a blocked-up window. The point cloud is coloured with the true colour acquired by the camera.

In the case of photogrammetric systems, point cloud reconstructions are not scaled to real (i.e. metric) dimensions. To correct this and also geo-reference the data, the second survey network presented in Section 3.3.1 is used. The eight targets attached to the walls are manually identified in the reconstructed point cloud and matched to the tie points, and a least square optimisation is conducted to deliver the best alignment possible. The resulting mean residual errors are summarized in Table 12 and range from 1cm to 3cm.

Table 12: Residual errors for the geo-referencing of the Nikon camera data.

Target Constraint	Data Source	Data Source	Error [mm]
T0	Total Station	Point cloud	31.7
T1	Total Station	Point cloud	20.6
T2	Total Station	Point cloud	12.1
T3	Total Station	Point cloud	34.9
T4	Total Station	Point cloud	13.1
T5	Total Station	Point cloud	18.7
T6	Total Station	Point cloud	16.6
T7	Total Station	Point cloud	11.3
Mean			**19.8**

3.3.5 PG 2 | UAV-Mounted Sony Alpha-7R

The UAV mounted with the Sony Alpha-7R camera was piloted by Cyberhawk Innovations professionals, aiming to take pictures at various heights around the garden. 460 pictures were acquired from locations slightly closer to the walls than in the previous case. As can be observed in Figure 18, the images appeared to cover all garden walls, in particular the rampart wall.

All the 460 pictures have been processed by Agisoft PhotoScan, delivering a dense point cloud containing 34 million points overall, including 20 million points for the rampart wall section. An orthophoto of the rampart wall and a close-up detail of a blocked-up window are shown in Figure 19. Again, it is interesting to note that the colours are brighter and generally appear more realistic than those obtained using the Faro scanner (Figure 15).

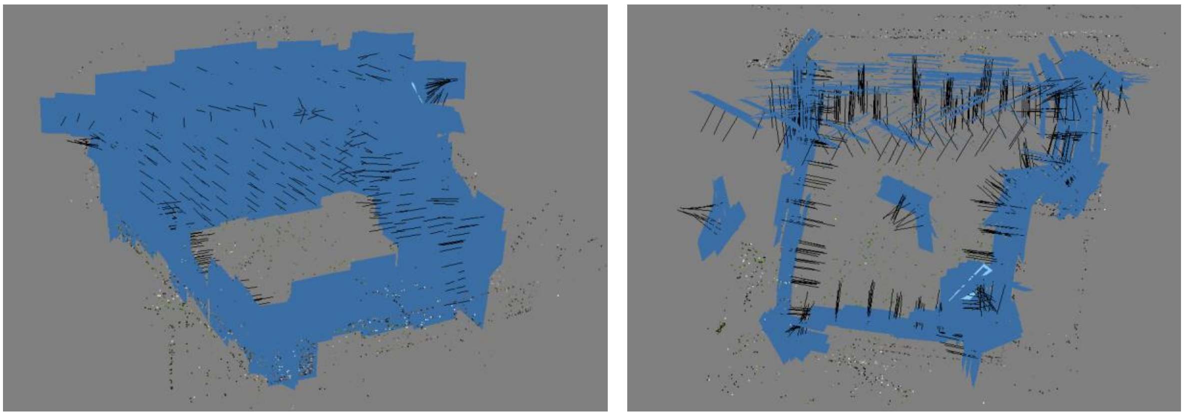

Figure 18: Camera positions and camera planes for the UAV system. Perspective (left) and top (right) views.

Figure 19: Main wall of the East garden obtained by the Sony camera. Right: detail of a window.

To correct the lack of adequate scale in native PG reconstruction and also to geo-reference the data, the survey network presented in Section 3.3.1 is used. The eight targets attached to the walls are manually identified in the point cloud and matched to the tie points, and a least square optimisation is conducted to deliver the best alignment possible. The resulting mean residual errors are summarized in Table 13 and range from 1cm to 3cm. These results are similar to those obtained for the PG 1 data.

Table 13: Residual errors for geo-referencing of Sony camera data.

Target Constraint	Data Source	Data Source	Error [mm]
T0	Total Station	Point cloud	28.6
T1	Total Station	Point cloud	14.7
T2	Total Station	Point cloud	7.4
T3	Total Station	Point cloud	24.7
T4	Total Station	Point cloud	21.1
T5	Total Station	Point cloud	19.8
T6	Total Station	Point cloud	13.6
T7	Total Station	Point cloud	14.9
Mean			**18.1**

3.3.6 PG 3 | Pole-Mounted Stereo-Camera System

The PG 3 system was mounted on the same carbon-fibre pole as the PG 1 system (see Figure 20) to reach higher part of the rampart wall – up to 5m.

With the objective of creating a 3D point cloud of the complete wall, more than 1,300 pairs of video frames were recorded at 1s intervals. However, a large number of these pictures were later removed because of their low quality (low exposure or motion blur). It is important to note that industrial cameras, like the ones used in this system, are conceived to work under controlled environments; variations in the lighting conditions can significantly affect picture quality. In the end, less than 100 pairs could be properly aligned to generate a 3D point cloud. This fact, together with the moderate overlapping between the selected pairs of images unfortunately provided an unsatisfactory point cloud (see Figure 21), not anywhere comparable to the dense and precise point clouds obtained with the other TLS and PG systems.

Figure 20: SVV system mounted on a pole.

Figure 21: Point cloud of the rampart wall facing the East garden obtained by the pole-mounted stereo system.

As a result of the system employing cameras with insufficient for outdoor usage, it was felt inappropriate to further compare its performance against that of the other TLS and PG systems. However, with a view to assess the value of stereo-camera systems, a study has still been conducted to compare the PG reconstructions obtained using only one of the cameras of the stereo PG system (i.e. used as a single-camera PG) and the stereo PG system (see Section 3.4.5).

3.4 Data Analysis and Results

The performance of the different 3D survey systems (except PG 3) are assessed and contrasted using several quantitative and qualitative criteria, including:

- *Data Accuracy and Precision*: taking the Leica ScanStation P40 data as 'ground truth', (we assumed here that it was the most precise and accurate data, which is reasonable in light of the advertised and observed performance), the 'distance' of the other datasets to it is calculated. This 'distance' is investigated using two approaches: point cloud vs point cloud, and point cloud vs mesh. Section 3.4.1 explains the 'distance' metrics and reports the results obtained.

- *Data Completeness*: data density and uniformity on the rampart wall surface are studied and compared for all technologies. Section 3.4.2 reports these results.

- *Efficiency*: the time required for acquiring and pre-processing the data to obtain a unified geo-referenced dense 3D point cloud is calculated and compared for all technologies (except PG 3). Section 3.4.3 reports the results obtained.

The comparison of the methods with respect to data accuracy and completeness is not undertaken using the entire East garden datasets, but with focus on the East rampart wall facing the garden. While some of the assessments are conducted using the data from the entire rampart wall, we also select three specific areas within it that are used to highlight the strengths and limitations of the different survey technologies. The three areas are shown in Figure 22.

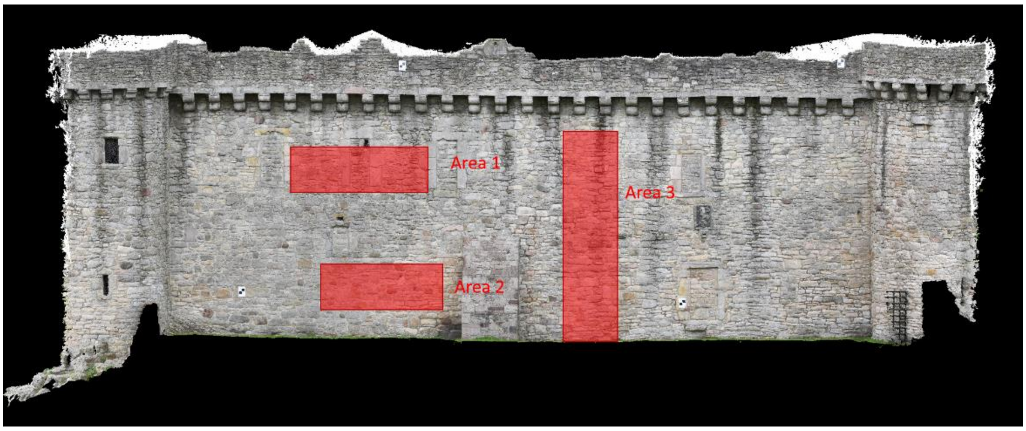

Figure 22: The three particular areas within the East rampart wall that are used for the performance assessment.

3.4.1 Data Accuracy and Precision

To analyse and compare the different datasets, one of them should be utilised as a reference. We selected the Leica ScanStation P40 laser scanning dataset (TLS 1) as reference dataset due to the expected (and observed) higher accuracy and precision of the device.

Once the data are geo-referenced and aligned, the Root Mean Square Error (RMSE) of the distance between each point in the other point clouds to the closest point in the TLS 1 point cloud is calculated. The results are summarized and illustrated in Table 14. These results further confirm the overall quality of the data acquisitions, reconstructions, alignment and geo-referencing, without any noticeable global error. The RMSE values are of the same order as the geo-referencing residual errors, which suggests that there is indeed no significant global error and that the observed deviations shall reflect the deviations in performance of the three 3D survey systems compared to the Leica ScanStation P40 scanner. In that regard, it already appears that, as would be expected, the Faro TLS point cloud best fitted the reference 3D data.

The RMSE metric above is not sensitive to noise and so may misrepresent performance. To achieve a more precise and accurate evaluation of the accuracy of the different 3D surveys, two different methods are considered that calculate the ‘distance’ of the other datasets to the P40 data (TLS 1). The first method is based on the comparison of the reference Leica ScanStation P40 point cloud with the point cloud obtained with the other method (Point cloud vs Point cloud – Section 3.4.1.1), whereas the second one is based on the Euclidean distance between the other point cloud and a reference mesh generated from the Leica ScanStation P40 data (Point Cloud vs Mesh – Section 3.4.1.2).

Table 14: RMSE and visualisation of the alignment of the Faro, Nikon and UAV data with the Leica data. Data in mm.

Faro (TLS 2) – Leica (TLS 1) RMSE: 3.7 mm	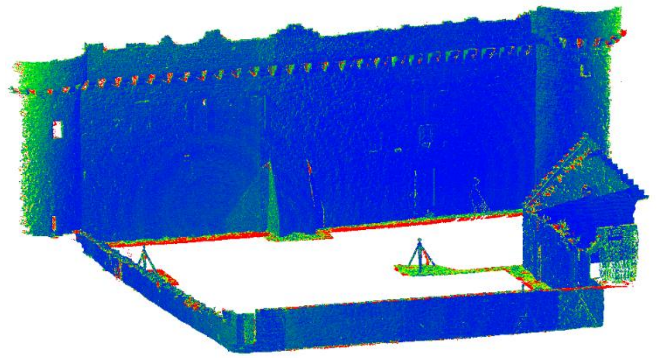
Nikon (PG 1) – Leica (TLS 1) RMSE: 9.18 mm	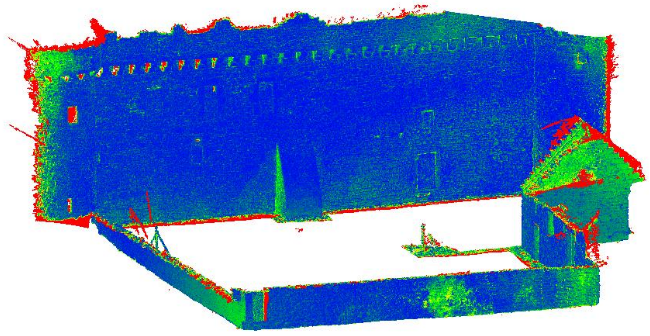
UAV (PG 2) – Leica (TLS 1) RMSE: 12.27 mm	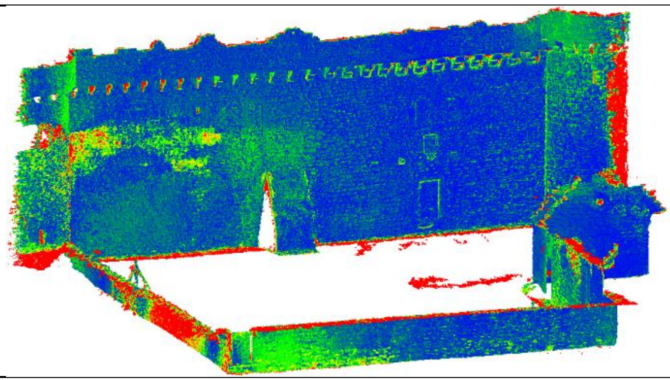

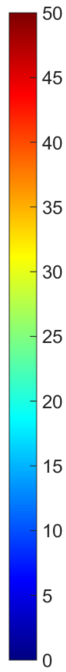

3.4.1.1 Point Cloud vs Point Cloud

This first approach computes the distance between two point clouds using the Hausdorff distance metric. For this, the volume containing the wall data is divided in voxels (i.e cuboids); we use voxels of size 1cm x 1cm x 10cm. The larger voxel side is the depth (perpendicular to the wall plane); it is set large to ensure matching points are found despite possible global misalignments). For each one of these voxels, the Hausdorff distance (d_H) between the two subsets of points A and B from the reference (Leica ScanStation P40) and the other datasets is calculated. The Hausdorff distance is defined as follows [44]:

$$d_H(A,B) = \max[d(A,B), d(B,A)] \quad (1)$$

where:

$$d(A,B) = \max_{a \in A} \min_{b \in B} \|a - b\| \quad (2)$$

Figure 23 illustrates the calculation of the Hausdorff distance. First (see first row), the Euclidean distance between each element of set A and each element of B is calculated. For each point of A, minimum distance is written and the arrow is coloured in green. Then (second row), the same computation is carried out from each point of B to each point of A. Finally, the maximum distances between sets are compared (highlighted in red) and the maximum value of these corresponds to the Hausdorff distance (highlighted in green in the third row).

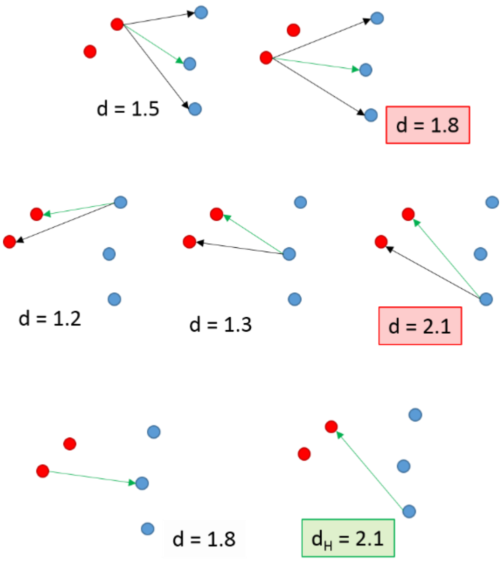

Figure 23: Hausdorff distance calculation for two datasets 1 (in red) and 2 (in blue). The first line illustrates the application of Equation (2) where A is the dataset 1 (red) and B is the dataset 2 (blue). The second line illustrates the application of Equation (2) where the datasets 1 (red) and 2 (blue) are inverted. The last line illustrates the application of Equation (1).

Note that this technique differs from standard point-to-point distance (for which the results are shown in Table 14), as it does not consider closest points in the two point clouds. Instead, it is based on the study of minimal and maximal distances between point clouds, which makes it more sensitive to noisy data (interestingly, it also makes it sensitive to variations in the uniformity of the cloud point density).

Figure 24 illustrates the results of the Hausdorff distance calculations for the three selected Areas of the rampart wall, and Table 15 summarizes the calculated mean Hausdorff distance and standard deviation for each case. As can be seen, the Hausdorff distance values are smaller for the Faro TLS with mean distances below 5mm in both Areas 1 and 2. The mean distance for the PG 1 reconstruction (pole-mounted Nikon camera) is only slightly higher and thus remains acceptable. The results are comparatively disappointing for the PG 2 reconstruction (UAV-mounted Sony camera), with mean distances between 10 and 20 mm. The results are particularly poor for Area 1. The reason behind this poor result is highlighted later in this report. In the case of Area 3, it is interesting to note the relative uniformity of the Hausdorff distance variations along the height of the wall for the PG 2 data which highlights the advantage of that system (UAV) in terms of access. For the pole-mounted Nikon system, the mean values increase more significantly at the bottom, because fewer images were taken of the lower parts – the operator was focused on the coverage of the upper part of the wall that is less reachable and did not think that an insufficient number of images would be taken for the lower part (e.g. taking pictures while on their knees).

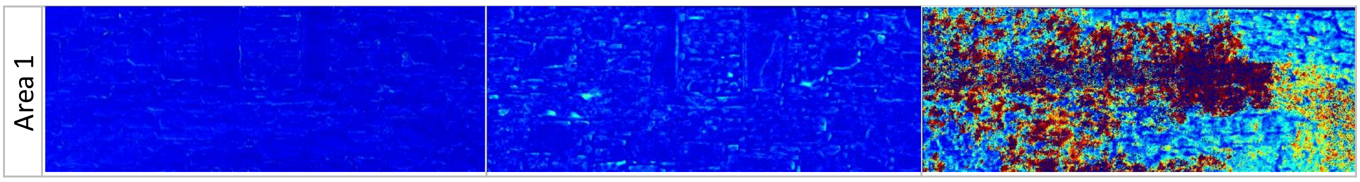

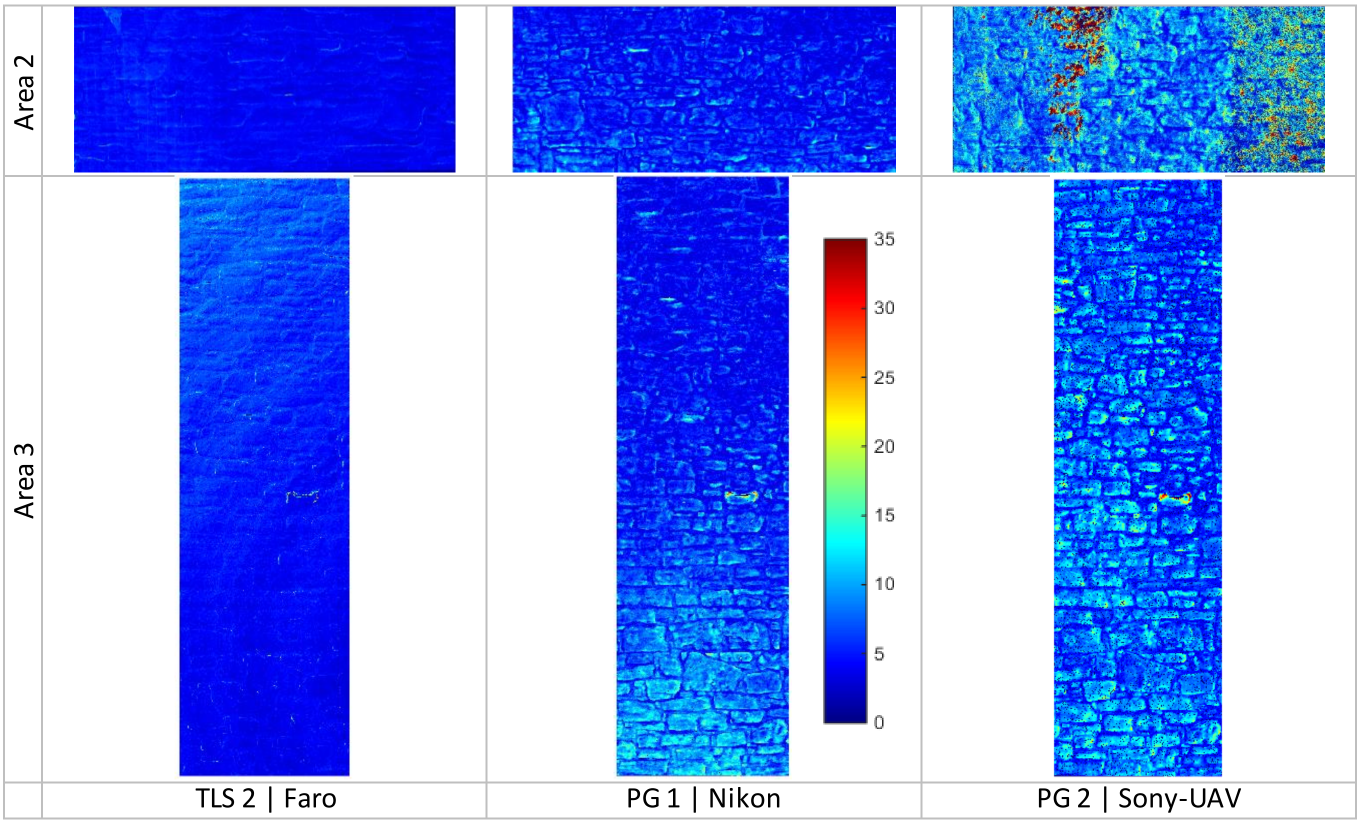

Figure 24: Hausdorff distance between Leica ScanStation P40 point cloud and the point clouds of Faro, Nikon and Sony for the three selected Areas of the rampart wall. Data in mm.

Table 15: Hausdorff distance and standard deviation (green) for the comparisons of the Faro, Nikon and Sony-UAV point clouds against Leica's point cloud, for the three Areas selected on the rampart wall.

Mean Hausdorff distance [mm] *Standard deviation [mm]*	**Area 1**		**Area 2**		**Area 3**	
Leica vs. Faro (TLS 2)	3.67	*1.06*	4.29	*0.99*	5.23	*1.66*
Leica vs. Nikon (PG 1)	4.36	*1.60*	5.09	*1.95*	6.14	*2.8*
Leica vs. Sony-UAV (PG 2)	17.62	*10.18*	10.79	*5.62*	7.76	*3.04*

3.4.1.2 Point Cloud vs Mesh

The second data precision assessment method is based on the calculation of the Euclidean distance between points in the other point clouds and a mesh reconstruction from the Leica's point cloud.

The mesh of the rampart wall has been created from the oriented Leica cloud points using Meshlab v.1.3.3, following the Poisson Surface Reconstruction method [45] at octree depth 11. Figure 25 shows the generated mesh along with the three study areas.

Figure 25: Mesh of the rampart wall. The three areas of interest are marked in blue.

Then, the distances between the point clouds and the mesh are calculated as the vertically-projected distances between each point and the mesh. Note than some small errors can appear in the generation of meshes. Therefore, the distance between the Leica ScanStation P40 point cloud and the mesh generated from it is also considered and subtracted from the cloud-to-mesh distances.

Figure 26 illustrates the distances between point clouds and mesh, and Table 16 summarizes the calculated average distances. These results (unsurprisingly) generally confirm those obtained earlier. The Faro point cloud appears very similar to the Leica, with points on average under 3mm from the Leica mesh. The point cloud generated by the pole-mounted Nikon camera shows similarly good, albeit slightly lower, precision. In fact, the mean value for the Area 3 is slightly lower for the photogrammetric reconstruction – but the standard deviation is always significantly smaller for the TLS demonstrating its overall superior precision.

As discussed earlier, it is interesting to note the homogeneity of the errors for the UAV reconstruction of Area 3 in contrast to what is achieved by the other methods.

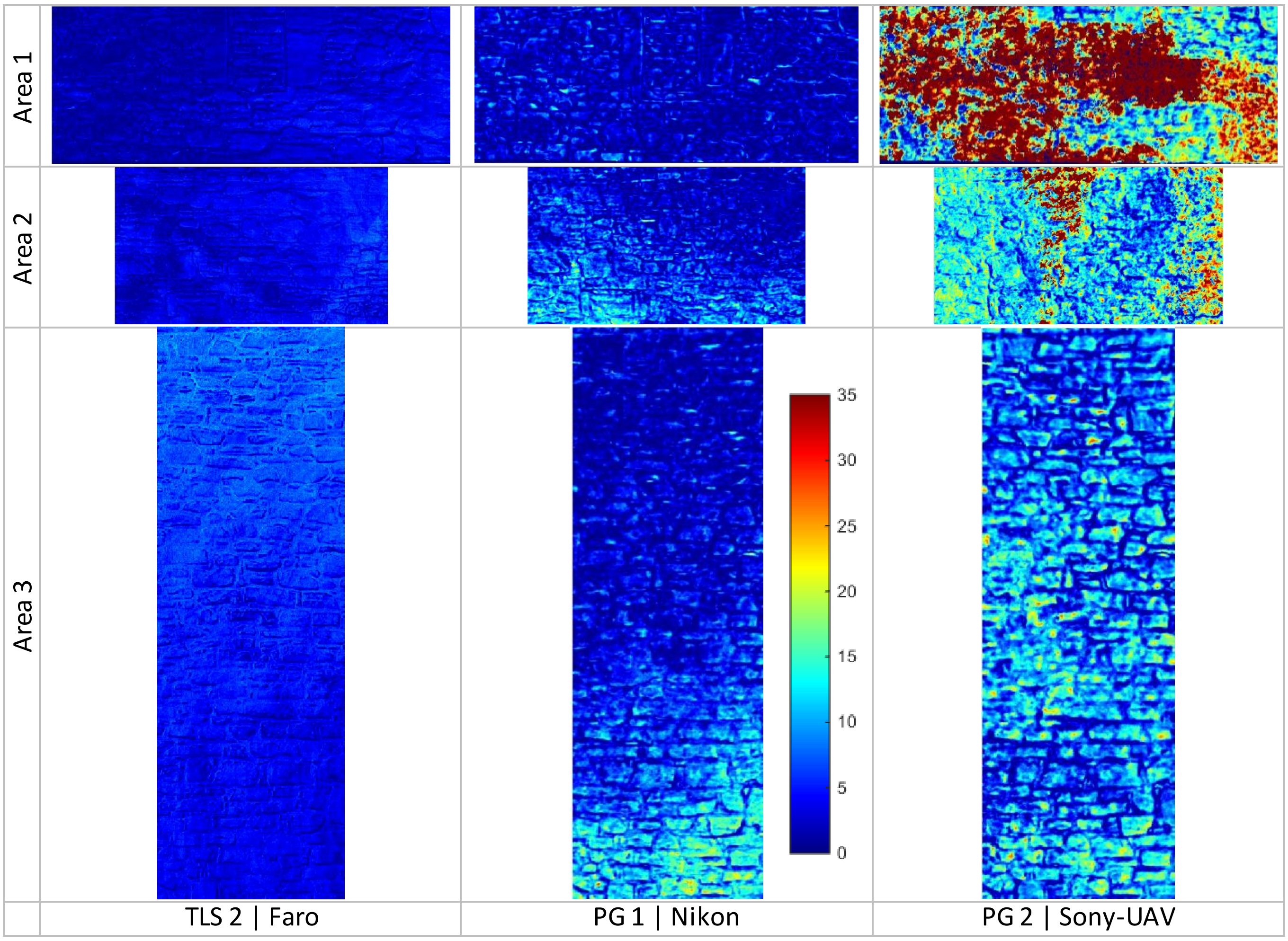

Figure 26: Point-to-Mesh distance between Leica ScanStation P40 mesh and point clouds of Faro, Nikon and Sony for the three selected Areas of the rampart wall. Data in mm.

Table 16: Mean distance and standard deviation (green) for the regions of interest.

Mean distance [mm] *Standard deviation [mm]*	**Area 1**		**Area 2**		**Area 3**	
Faro	1.3	*0.85*	1.9	*0.95*	2.9	*1.2*
Nikon	1.3	*1.2*	2.6	*2.1*	2.8	*2.6*
UAV	15.9	*10.4*	8.0	*5.2*	4.7	*2.8*

3.4.2 Data Completeness

The previous results illustrate how TLS devices provide more precise and accurate results than photogrammetric systems, with the pole-mounted Nikon system (PG 1) nonetheless demonstrating comparatively good results. But, performance cannot be solely judged upon data precision and accuracy. Another important criterion is data completeness, that assesses data point density and uniformity. In this subsection, data density and uniformity along the rampart wall of the garden are compared for the different systems.

Table 17 illustrates the difference between point clouds in terms of point density. Point density is calculated by projecting the reconstructed points on the wall plane and then calculate the density of points within that plane. As can be seen, the density is higher for the laser scanners, but there is no significant difference between the Faro TLS (TLS 2) and the Nikon PG (PG 1) systems.

Table 17: Density-related parameters for the obtained point clouds.

Survey System	Max density [pts/cm^2]	Mean density [pts/cm^2]	Standard deviation [pts/cm^2]
TLS 1 | Leica	164	75.94	11.67
TLS 2 | Faro	49	22.99	3.88
PG 1 | Nikon	31	16.09	3.05
PG 2 | Sony-UAV	23	7.54	2.29

Data density and its uniformity are clearly illustrated in Figure 27 for Area 3. This figure shows the (relative) density of points in each squared centimetre with respect to the maximum value. A clear vertical gradient of density is observed in the TLS datasets. On the upper end of the wall, the top part of the stones (and the mortar joints above those) is clearly incompletely scanned due to (self-) occlusions resulting from more prominent stones. In contrast, data density is more homogeneous for the photogrammetric systems.

This highlights a key limitation of TLS over PG. The lack of portability of laser scanners leads to situations where laser scanners quickly loose line of sight. Addressing such issue would require the utilisation of complex and costly access solutions (e.g. scaffolding) that would still need to be sufficiently stable to ensure reliable laser scanning operations. In contrast, the possibility to mount digital cameras on poles or UAVs can make PG systems usable in many more contexts without the need for costly access provision.

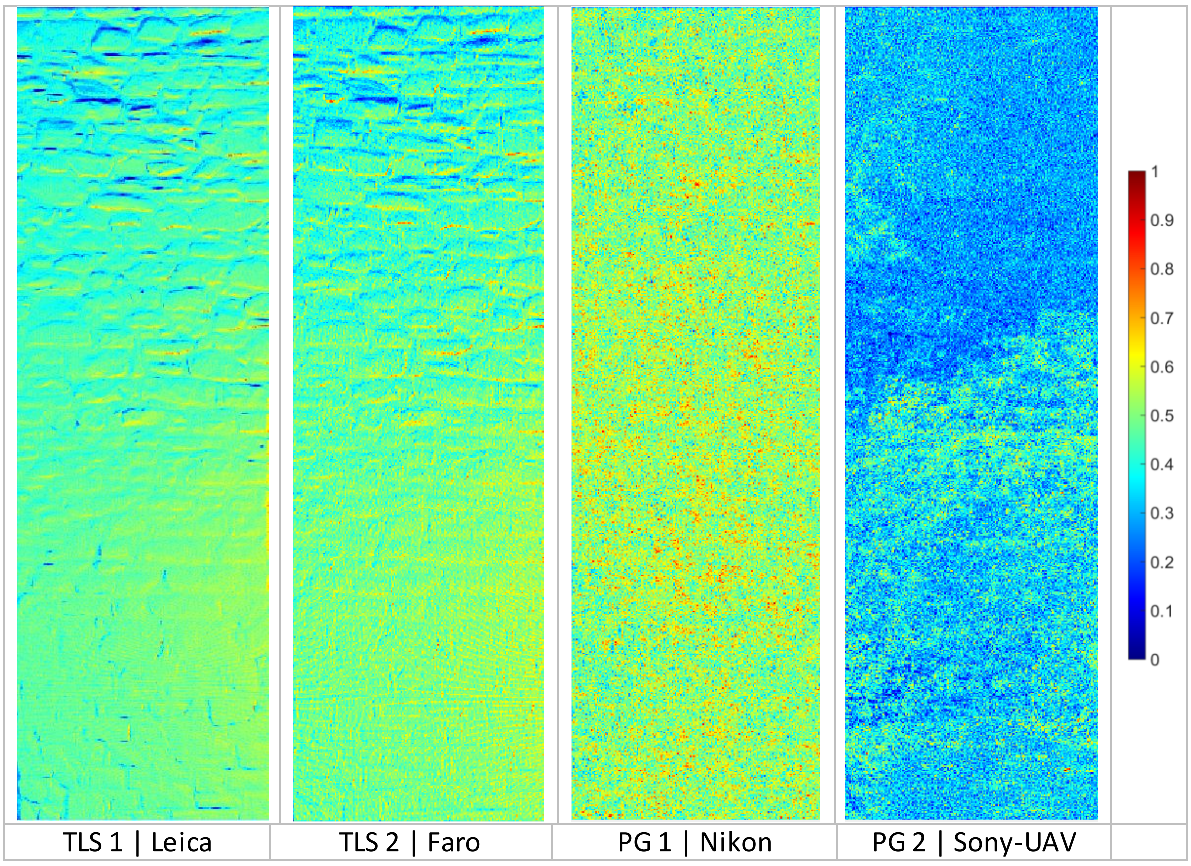

Figure 27: Uniformity of point density along the Area 3 of the main rampart wall.

Figure 28 shows close-ups of the point clouds for the top parts of Area 3. While this figure further illustrates the uniformity of point density for the four systems, it is interesting to note that, in the case of the Leica ScanStation P40, this could also be in relation to what is commonly known as *edge effect* (see how upper parts of several stones are not recorded). This result is surprising considering the overall performance of the scanner, and can be due to two different reasons. Either the Leica ScanStation P40 does not effectively handle edge effects, or the scanner employs a very stringent criterion to reject potential spurious points resulting from edge effects (to reduce the risk of false positive errors). The seemingly good results obtained with the Faro Focus 3D scanning tend to favour the first reason, but these results are not sufficient to provide reliable conclusions on the subject.

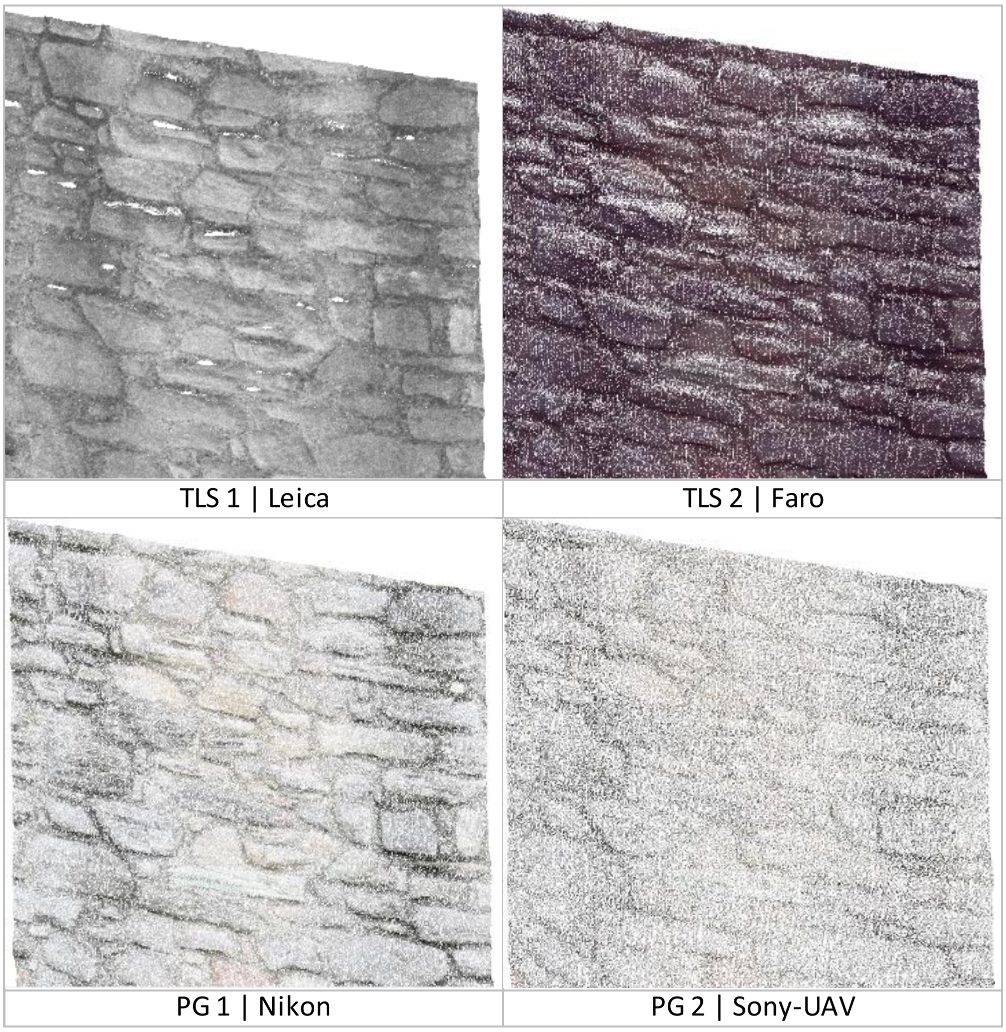

Figure 28: Points clouds of the top part of Area 3.

3.4.3 Efficiency

An additional criterion for comparing performance between TLS and PG systems is efficiency. This is defined as the time required for acquiring and pre-processing the data to obtain a unified geo-referenced dense 3D point cloud. Acquisition time comprises the positioning of the devices around the garden and the acquisition of data (for TLS devices) or pictures (in the case of PG systems). Pre-processing includes data transfer, registration/geo-referencing, colourisation (for TLS 2) and data cleaning (removing spurious data).

Table 18 shows the estimated time recorded for each task for each survey system. Note that the pre-processing operations have all been undertaken on the same computer (i7 3.60GHz processor and 12 GB RAM).

Regarding the acquisition stage, the scanning time appears significantly shorter for the Leica than for the Faro TLS. But, this is essentially due to the fact that no colour information was acquired during the Leica scanning (the Leica ScanStation P40 scanner may still be slightly faster, but not significantly). An important difference is also noticeable between PG 1 and PG 2. This is due to two factors. First, due to the longer focal length selected for the PG 2 system, many more images had to be acquired. Secondly, the UAV could only work for 10-minute periods at a time, after which the

UAV had to be landed to change its battery before resuming works. Combined, these two factors resulted in a significantly longer acquisition time than anticipated. As discussed later, selecting a lens with a shorter focal length would reduce acquisition time without impacting reconstruction quality.

Pre-processing times are similar for all systems, despite the fact that they require different tasks. The main observation is that pre-processing times are in this case study often more than double acquisition times, despite the use of a high-performance computer. This contributes to the overall findings presented in which a shift in the efficiency restriction to conduct 3D surveys is occurring from data acquisition to data processing.

Table 18: Acquisition and pre-processing times for TLS and PG systems.

Survey System	Acquisition	Pre-processing	Total time
TLS 1 | Leica	40min	3h	3h 40min
TLS 2 | Faro	1h 30min	2h 30 min	4h
PG 1 | Nikon	30min	3h 15min	3h 45min
PG 2 | Sony-UAV	1h 30min	3h 15min	4h 45min

3.4.4 PG 1 vs PG 2

As has been shown in previous subsections, reasonably good quality results can be achieved with PG systems. However, local variability in the quality of the reconstruction has highlighted that some parameters can particularly affect the performance of those systems: (1) camera locations, and (2) camera properties and settings. These parameters impact the overlapping between the pictures, which is critical to the external calibration of the images, and subsequently to the quality of the 3D reconstructions.

PG 1 and PG 2 actually used different camera setups and camera positioning methods, which we believe cumulatively explain the poorer results achieved by PG 2 (Sony-UAV).

Table 19 shows that the camera settings of PG 1 and PG 2 differed in several ways. First, the UAV did not use entirely manual settings which led to images with varying ISO and F-stop values. But, an important difference is in the lens's focal length. The focal length of PG 2 is 3 times larger than the one used on the Nikon, which implies that the wall area covered by each picture was significant smaller. To ensure a sufficient amount of overlap between pictures, a significantly larger number of images should have been acquired. Although twice more pictures were acquired using the PG 2 system compared to PG1, this appears not to have been sufficient. Indeed, the poor quality of the reconstructions achieved in the local areas of the rampart wall Area 1 and Area 2 shown in Figure 24 and Figure 26 directly correlates with a lower overlap between images acquired with the UAV in these areas, as can be seen in Figure 29 (top). Figure 29 shows the variability in the density of images acquired by the UAV (top) in contrast with the Pole-mounted Nikon system (bottom), which in addition to the difference in focal lens, significantly impact the final results.

The PG 2 system operators may have expected that, by acquiring more images with a lens having a longer focal length, better results would be produced. But, they underestimated the full impact of a longer focal length on the number of images needed to be acquired. In this case, it seems that they should probably have acquired twice more pictures (which would have further negatively influenced the acquisition time discussed in Section 3.4.3). Naturally, other factors may have influenced the results, such as the variable F-stop and ISO values. However, we would like to note that the PG 2 pictures did not seem to show motion blur and other signs of lower quality compared to the pictures acquired with the pole. This suggests that, thanks to their modern gimbals, UAVs can provide a reliable platform for the acquisition of images for photogrammetric purposes.

Overall, it appears that the 14mm focal length and image density employed with the PG 1 system were quite adequate for pictures acquired at 5m. An important lesson is that careful planning should be considered to select the appropriate picture density (and locations) for the given camera settings. This process may be referred to as: *Planning for Photogrammetry (P4P)*.

Table 19: Properties and settings of the cameras used in the two PG systems.

PG System	Size [px]	N. of pictures	Focal length [mm]	F-stop	ISO	Shutter [s] (Exposure)
PG 1 | Nikon	7360x4912	~260	14mm	f/8	250	1/125
PG 2 | Sony-UAV	7360x4912	~460	35mm	f/4-f/8	100-400	1/500

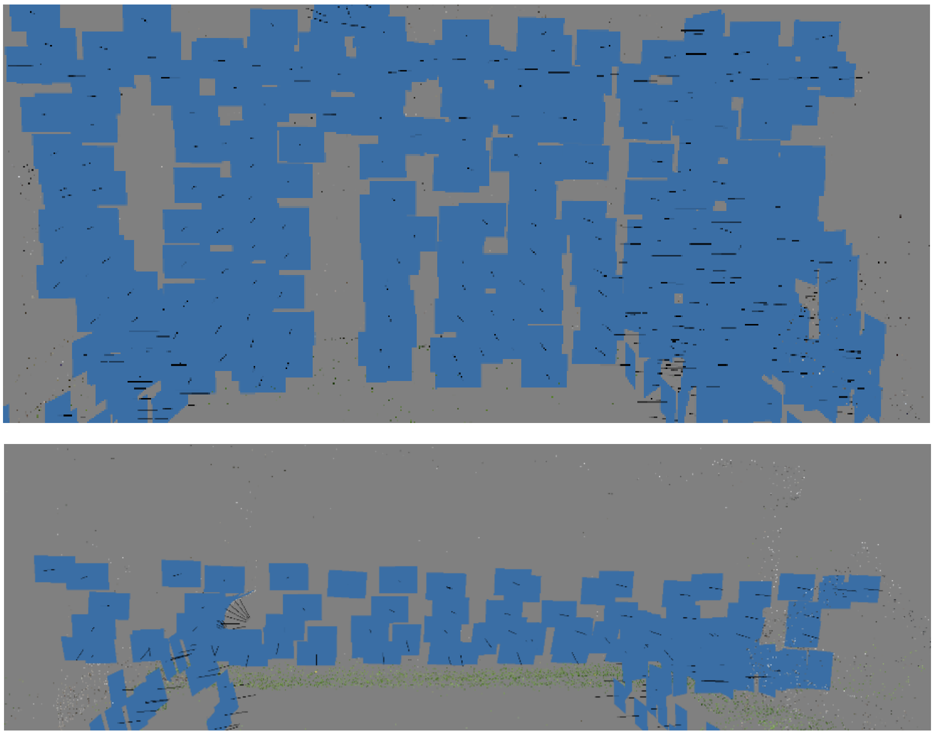

Figure 29: Camera locations for UAV (top) and pole mounted (bottom) data acquisition.

3.4.5 Stereo-Camera Photogrammetry

As previously indicated, the stereo-camera PG system (PG 3) did not use cameras with sufficient quality to deliver reconstructions in any way comparable to those obtained by the other systems. Nonetheless, a study can be conducted to assess the gain in quality that a stereo-camera PG system could provide compared to a single-camera one, by using the data provided by the Stereo-camera PG system (PG 3) alone.

With stereo-image PG systems, the identification of common feature points is more robust due to the broad overlapping and known external calibration between pairs of synchronised pictures, which leads to better depth estimations. To study the differences between a single-camera PG dense reconstruction and a stereo-camera PG dense reconstruction, two parts of the main rampart of the

East garden were analysed: an area around a blocked-up window on the wall (‘window’), and a corner area at the intersection of the wall and the corner tower (‘corner’).

3.4.5.1 Window

The first of the studied regions is shown in Figure 30 and corresponds to a flat section of the rampart wall containing a blocked-up window and a vent above it. Four synchronised pairs of pictures were taken with the left and right cameras at 5 meters from the wall (see Figure 31) and three point clouds were generated: one point cloud using all calibrated pairs of images (i.e. stereo-camera reconstruction) and two point clouds generated using the left and right pictures separately. Both left and right cameras have parallel epipolar lines and the distance between them is known and is equal to 38 cm. These constraints can be seen in Figure 31(c), where the baselines are marked in yellow.

Figure 30: Area around a blocked-up window.

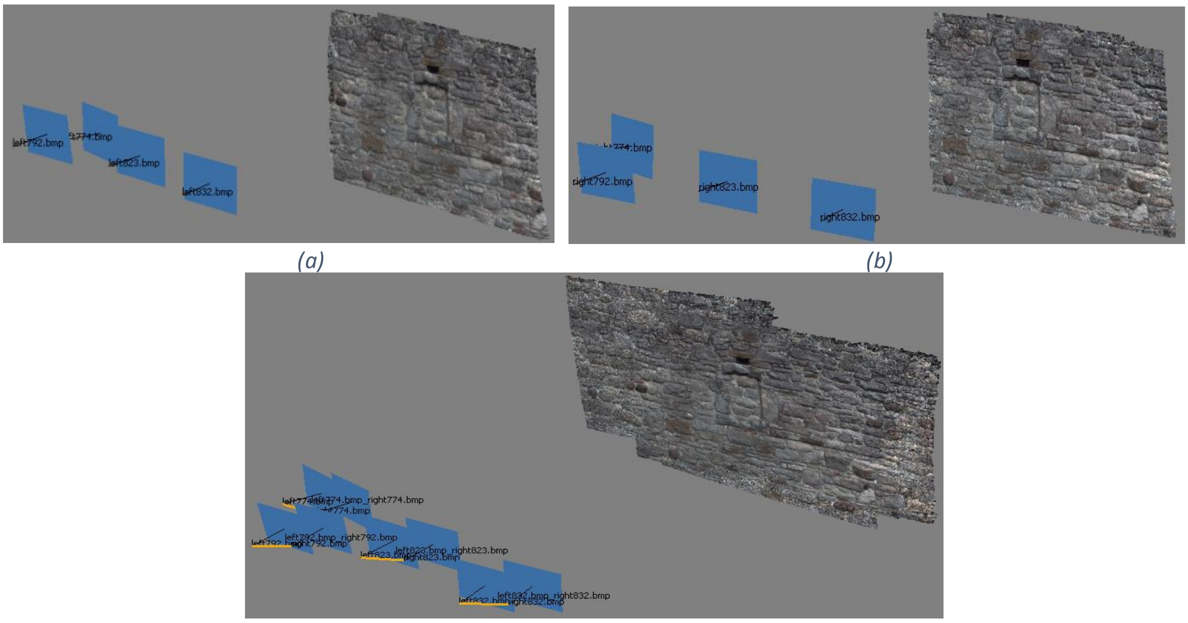

(a) (b)

(c)

Figure 31: Location of cameras and point clouds generated by left camera pictures (a), right camera pictures (b) and stereo pairs of images (c) in the ‘window’ area.

We have then compared the three point clouds to the reference data delivered by the Leica ScanStation P40 TLS (TLS 1). Note that survey networks are not properly digitised in these experiments. As a result, the alignment of the TLS and Photogrammetric data was achieved by manually selecting matching points in both datasets.

As can be seen in Figure 32 and in the statistical information summarised in Table 20, the errors are quite similar for all three reconstructions in this area, with a mean distance is around 5mm and standard deviation under 4mm, with the error appearing more ‘balanced’ in the stereo system.

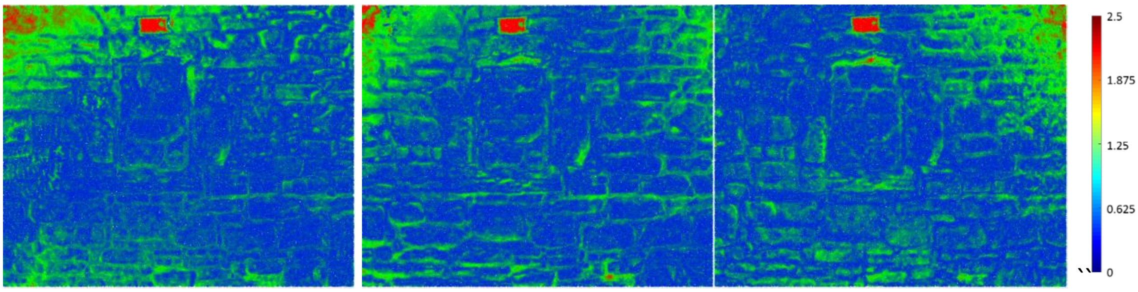

Figure 32: Difference between point clouds from the left camera (left), right camera (right) and stereo system (centre) and the TLS data for the window area. Data in cm.

Table 20: Mean distance between points, standard deviation and median values for point clouds compared to TLS data.

Camera System	Mean [mm]	Std. deviation [mm]	Median [mm]
Left camera	5.2	3.4	4.4
Right camera	5.4	3.7	4.4
Stereo system	5.2	3.4	4.3

3.4.5.2 Corner

The second studied region is a corner at the intersection of the main rampart wall and one of the circular towers (see Figure 33). In this case, ten synchronised pairs of pictures were taken by the stereo-system at 3-4 meters from the wall, as shown in Figure 34.

Figure 33: Area between the main wall and a tower.

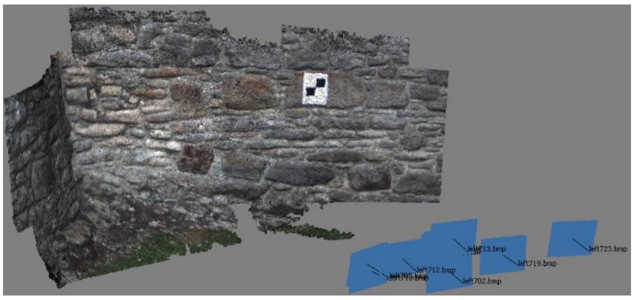

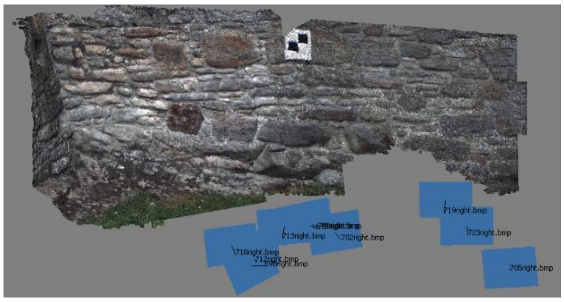

(a) *(b)*

(c)

Figure 34: Location of cameras and point clouds generated for the left camera pictures (a) the right camera pictures (b) and the stereo system (c), for the 'corner' case.

Baseline and cameras orientation information is considered to create a point cloud from all stereo image pairs. However, as Figure 34(c) illustrates, several pairs of images have had to be discarded and only 4 pairs were used to create the point cloud (as a result of the inadequacy of the cameras for this kind of environment, and also the sub-optimal calibration of the left camera identified post-survey). The reduced number of images used for the stereo reconstruction explains the smaller region reconstructed compared to those generated by means of the individual cameras.

The distance between each point cloud and the reference data from Leica were calculated in the same way as for the 'window' region. The results are shown in Figure 35 and Table 21. Significant differences between the reconstructions are this time visible. The mean distance between points is almost 40mm for the left camera whereas this value is 12.1mm for the stereo reconstruction. On the other hand, the reconstruction for the right camera is only slightly worse than that of the stereo reconstruction.

These results are difficult to interpret. Indeed, it was identified post-survey that the left camera had not been optimally calibrated. As a result, although the stereo-system seems to produce better results than each individual set of images, no reliable conclusion can be drawn from these experiments, and further work should be conducted to ascertain the enhanced performance of stereo cameras. In particular, the accuracy in the scaling of the data automatically achieved by stereo-camera PG systems needs to be studied using a better system.

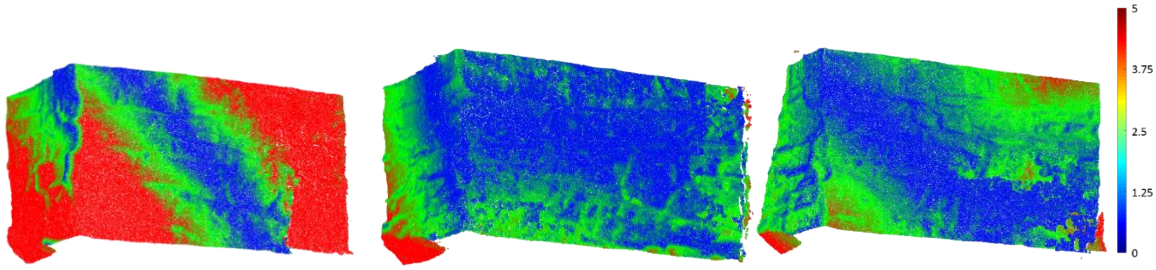

Figure 35: Difference between point clouds from the left camera (left), right camera (right) and stereo system (centre) and the TLS data for the corner area. Data in cm.

Table 21: Mean distance between points, standard deviation and median values for point clouds compared to TLS data.

Camera System	**Mean [mm]**	**Std. deviation [mm]**	**Median [mm]**
Left camera	39.2	26.6	37.0
Right camera	14.5	10.6	13.0
Stereo system	12.1	11.6	8.6

3.5 Summary

Terrestrial laser scanning and photogrammetry are increasingly used for building surveying, providing dense textured 3D point clouds and meshes. In terms of geometry, data from TLS are particularly accurate. While this is not surprising and was anticipated, in the case study considered here the Faro Focus 3D scanner point clouds were close to the Leica ScanStation P40 ones. This similarity is interesting, although it must be remembered that these results are obtained at rather short ranges (maximum 10m) and the performance of the Faro scanner would be expected to deteriorate significantly faster at larger distances.

While TLS clearly provides good geometric data to generate accurate and valuable 3D models, it also has three important limitations. First, TLS devices are relatively expensive (tens of thousands of pounds per unit; although the price has decreased rapidly in the last decade). Then, the cameras embedded within the scanners do not produce good quality colour information compared to what is achieved with common DSLR cameras. And finally, but still very importantly, current TLS devices have to be operated from stable positions, which reduces their mobility and the range of contexts within which they can be reliably employed.

In contrast, modern digital cameras are relatively cheap and very portable, making them suitable for a wider range of contexts. However, their main limitation is their variable performance depending on the level of texture in the scene being reconstructed. Nonetheless, scenes like the stone wall case study considered in this work present great textures for the application of photogrammetry. In such contexts, photogrammetry can be a realistic alternative to terrestrial laser scanning.

Mounting a camera on a UAV can further solve access issues. A copter-type UAV can fly around close to buildings and take pictures from different viewpoints without the need for any additional infrastructure (e.g. scaffolding). This theoretically makes this solution usable in more contexts, enabling reconstructions with more predictable quality (e.g. without occluded areas, as was shown with TLS).

4 From Data to Information, Visualisation and Decision Making

The review of the literature on reality capture, data processing and management technologies in the AEC/FM sectors clearly shows that these novel technologies offer great potential for surveying and managing historic monuments. Novel sensing technologies, like TLS and PG, information and communication technologies, like cloud services, virtual and augmented reality, and the development of BIM processes will altogether transform current practice surrounding the management of and public engagement on historic monuments. The authors also believe that the technologies will facilitate the development of pro-active maintenance schemes for historic monuments.

The literature review, and the results reported in Section 3 go some way to confirm this, showed that reality capture technologies have progressed dramatically in the last decade, so that large amounts of accurate data can now be attained relatively rapidly. This means that a traditional significant barrier to the effective and efficient survey of historic monuments, that is the acquisition/recording of reliable data from the monuments, has now been significantly alleviated. Yet, this (r)evolution in reality capture technology has not yet resulted in their widespread adoption. The literature review and our own experience indicate that this progress actually only revealed that processing of the acquired data is now the new barrier to effective and efficient surveys. For stone masonry surveys, the literature showed that analysis of 3D data to extract the information that is actually valuable to surveyors and other heritage experts is still essentially undertaken manually, with 'visual' evaluation (e.g. segmentation of walls into different areas and measurement of those areas, for example for presenting and estimating the amount of repair) still being prevalent. Such processes are time-consuming, are often costly due to expert's time being utilised. Additionally concerns surround the subjectivity and resulting variability of assessment and reporting. There is thus a growing need for efficient and effective methods to (semi-)automatically process data from modern reality capture technologies to facilitate the job of surveyors and heritage experts and enable them to focus on more value-adding activities such as conducting building pathology from identified defects, and development of in-depth repair strategies.

The remainder of this section reports preliminary results from on-going works that aim to demonstrate that computer algorithms can be developed that can automatically extract 'first-level' information from TLS and PG survey data, information that is of particular relevance to the work of surveyors. In particular, we have developed a computer system for the analysis of textured 3D point clouds of rubble stonewalls, acquired using TLS or PG. The system is aimed at automatically segmenting the data into their individual stones and mortar joints; this segmentation/labelling can then support the extraction of further information of value to surveyors. For example, focusing on mortar joints, the system can report the mortar linear distance and the depth profile along the mortar lines that constitute important information to accurately estimate the quantity of repointing to be undertaken. The system can also automatically estimate the amount of pinning that should be included based upon the maximum joint width.

Detailing the algorithm for the segmentation of masonry is beyond the scope of this report. That said, the reporting and analysis of the results obtained contributes to support the idea that well-crafted algorithms can constitute powerful tools to support surveyors in their work, enabling them to achieve higher levels of survey completeness, objectivity and efficiency. We do not suggest that such algorithms could in any way replace surveyors altogether. Instead, we argue that they can reduce the amount of pain-staking, and low value-adding tasks currently conducted by surveyors (e.g. measurements), thereby freeing time for them to focus on value-adding tasks, such as defect analysis and the development of repair strategy. In addition, it is envisaged that these techniques will have a significant impact upon proactive maintenance programmes and broader building portfolio management.

4.1 Case Study

We present results obtained for a section of the Craigmillar Castle East garden rampart wall. The section, shown in Figure 36, is approximately 5m wide and 2.5m high, and has been selected for its overall level of complexity. Indeed, as can be seen in Figure 36 (right), this wall section presents varying textures resulting from rain water flowing through the machicolations at the top of the rampart. Furthermore, one can see an old window opening that has later been blocked up, which adds complexity in terms of the size, shape and pattern of the stones encountered. It is also important to note that the colours and textures of the stones and mortar regions of the wall are fairly similar, although not identical. All these characteristics make the segmentation process extremely challenging.

The results reported below are obtained using the Leica ScanStation P40 point cloud data.

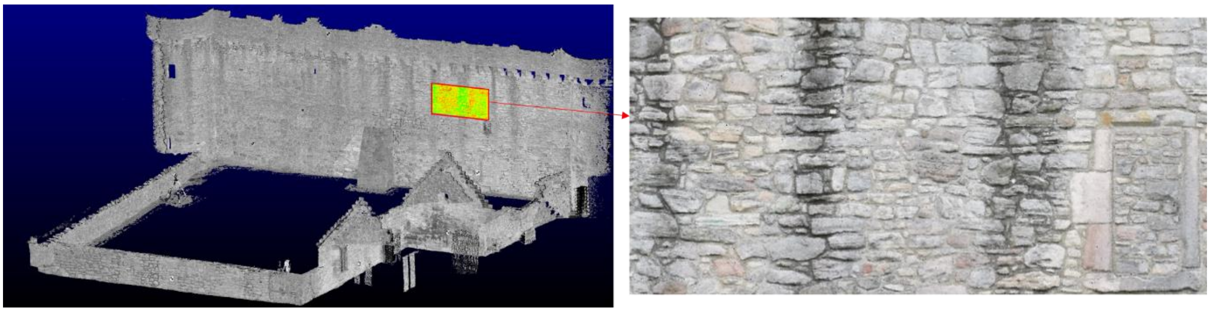

Figure 36: Textured laser scanned point cloud of the East garden. Left: the entire point cloud. Right: a zoom into a 5m x 2.5m section of the rampart wall.

4.2 Stone/Mortar Segmentation

We developed an algorithm that considers the 3D information globally and at local level, to segment the wall point cloud data into regions corresponding to individual stones and mortar joints. Without being overly detailed, the algorithm is based on the analysis of the data in the frequency domain, with mortar joints detected as 'narrow valleys'.

Figure 37 shows the results obtained for the selected wall section with each 'compact' coloured region being a detected stone. Notice how the algorithm effectively deals with stones and mortar joints of various shape and profile. Although some stones may at first appear to exhibit similar colours, these are actually different tones.

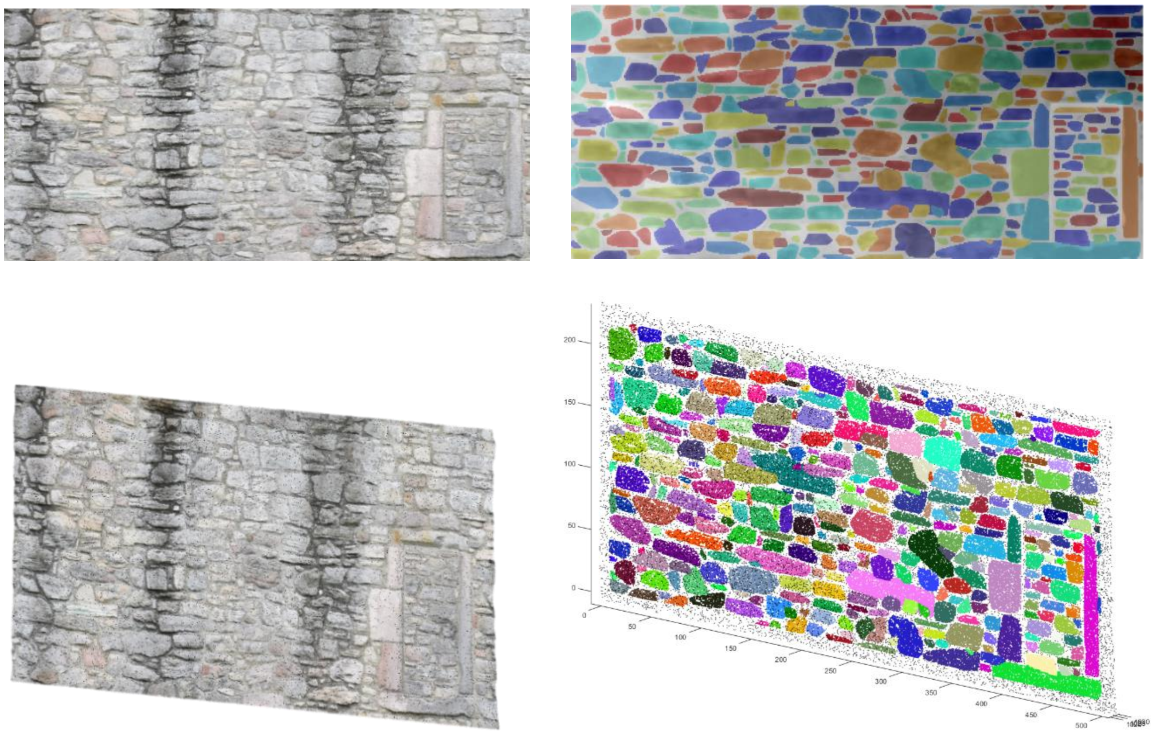

(a) (b)

Figure 37: Wall stone segmentation results. (a) shows an orthophoto and 3D view (point cloud) of the wall section; (b) shows the segmentation results in the same orthophoto and 3D view.

A quantitative assessment of the segmentation accuracy has been undertaken by comparing the results obtained by the algorithm against those obtained through a meticulous manual segmentation in the section's orthophoto. Figure 38(a) illustrates the labelling performance results. It shows good overall results, although the size of the stones seems slightly over-estimated by the current algorithm. Figure 38(b) further summarizes the results of Figure 38(a) by colouring each stone according to the percentage of its area in the orthophoto that is correctly labelled as stone. As can be seen, the area of most stones is typically well segmented, with ratios over 75% for the majority of stones. The few errors appear for some (but not all) of the smallest ones.

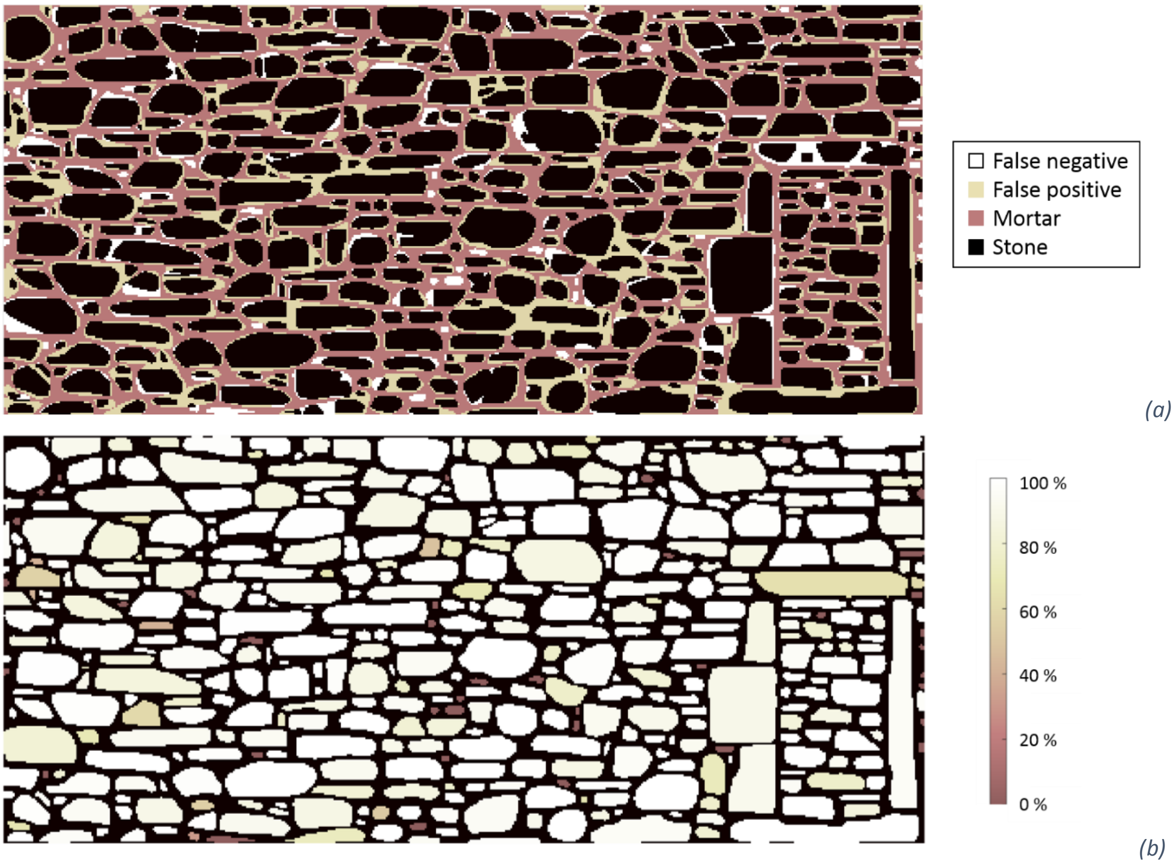

Figure 38: Illustration of the assessment of the performance of the proposed wall segmentation algorithm. In (a) the labelling performance results are shown. Black and magenta regions are pixels that are correctly recognized as stone and mortar respectively. Yellow regions are 'false positives', i.e. mortar areas that are incorrectly labelled as stone. White regions are 'false negatives', i.e. stone areas that are incorrectly labelled as mortar. In (b) each stone is coloured according to the percentage of its area (in the orthophoto) that is properly labelled as stone.

4.2.1 Curved Wall Sections

Many algorithms proposed to date to process 2.5D data have been experimented on data attained from flat wall sections. The reason is that they conduct their analysis by investigating deviations from the wall plane. Yet, not all walls are planar. While some are intentionally curved (e.g. circular towers), historic masonry walls that were designed and built planar now often present irregular, undulated surfaces (e.g. due to settlement or deformity). It is therefore of interest to have data processing methods that are robust to varying contexts and do not rely on strong assumptions such as overall wall planarity.

The method that we develop does not make such assumption, and is robust to local wall undulations as well as large (designed) wall curvatures. To demonstrate this, we applied our algorithm to a section of wall from the North-East tower of the castle. Figure 39 shows the location of the section that is approximately 3.5m high and 1.5m wide and has significant curvature, as shown in the section's top view.

Figure 40 shows the segmentation results obtained, with each 'compact' coloured region being a detected stone (although some stones may at first exhibit similar colours, these are actually different tones). Notice how the algorithm deals reasonably well with stones and mortar joints of various shape and profile despite dealing with a curved wall.

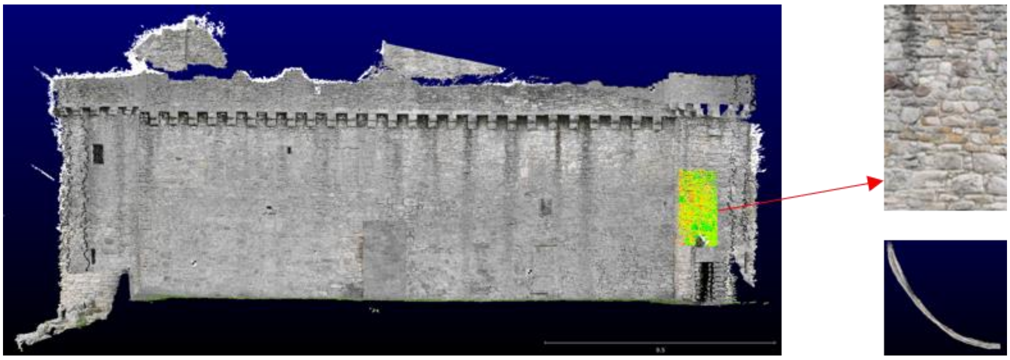

*Figure 39: Textured point cloud of the East garden. Left: the entire point cloud.
Right: Front and top view of the curved test section.*

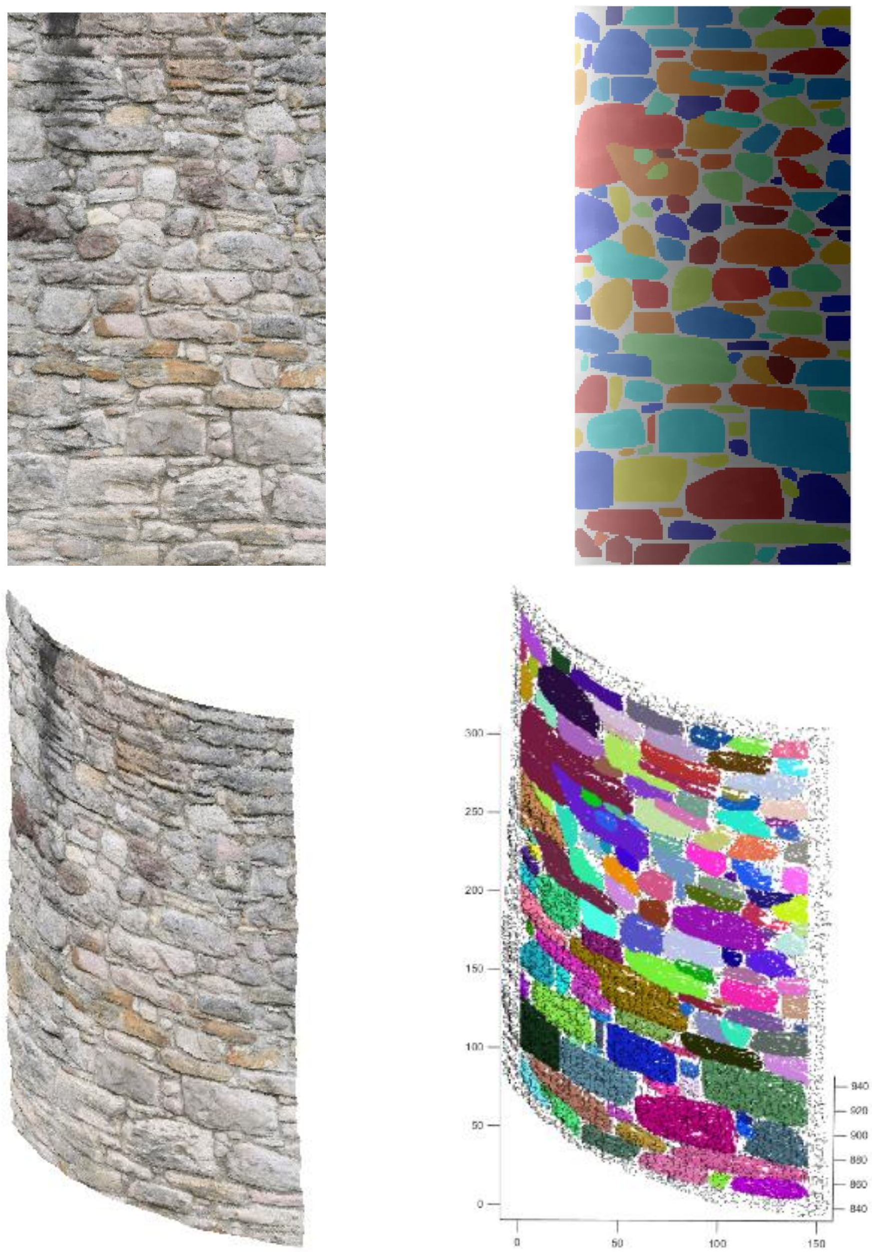

(a) *(b)*

Figure 40: Curved wall stone segmentation results. (a) shows an orthophoto and 3D view (point cloud) of the wall section; (b) shows the segmentation results in the same orthophoto and 3D view.

4.3 Study of Mortar Joints

The automated segmentation and labelling algorithm separates stones from mortar joints. While this can be useful on its own (e.g. to automatically track the movement or erosion of individual stones over time), additional analysis of these areas can provide further valuable information.

For example, the mortar joint data can be further processed to elicit recessed zones, and therefore the amount of maintenance works needed. Indeed, numerous wall repair processes are currently estimated on a square-metre (m^2) basis [46, 47, 48], which leads to significant approximations in repair costs. More precise repair work quantification and therefore costings would be obtained if more accurate measurement metrics were used, such as the length, depth and width of joint mortars. While such accurate measurement is too difficult to conduct manually (which is why square-metre approximations have been utilised), we demonstrate here that the point cloud data provided by TLS and PG can be automatically processed to obtain such measurements.

We have developed an algorithm to automatically measure the length, width and depth of mortar joints. Without going into detail, the algorithm aims first at detecting the mortar areas centre lines (skeleton) and then studies the depth and width of the mortar areas at all points along these lines.

Results for the selected rampart wall section are shown in Figure 41. From the centre lines (Figure 41(a)), the length of mortar joints in the wall can be obtained exactly. Here, the length is automatically calculated to be 110m, which compares with a length of 125m obtained from the manually segmented data. While this still shows a 12% error, this result is positive, particularly when set within the perspective of the complexity of the case considered here and contextualised within the current lack of objective method for conducting such measurements.

The depth of the mortar recess along the centre lines can also be automatically calculated which enables the detection of mortar areas that require repointing. Figure 41(b) shows the depth of the mortar regions along their centrelines. The more red a line, the more recessed the mortar joint in that area.

The width of the mortar joints along their centrelines can also be derived. This information, along with the depth and length of mortar joints would support the evaluation of the volume of mortar that would be required for repairs. Figure 41(c) shows the width of the mortar regions along their centrelines. The more red the line, the wider the mortar joint.

The knowledge of the width of the mortar can be also be used to automatically quantify the amount of pinning (or *gallets*) that should be necessary to repair a given wall. Indeed, traditional lime mortars cannot be used to fill large joints between stones due to excessive mortar shrinkage and subsequent failure; pinning stones are normally used to fill those large gaps prior to apply the mortar. Like other repairs, the quantity of pinning is traditionally derived approximately from the wall surface (square metres). Instead, we have developed a preliminary algorithm that further processes the results above to automatically detect likely locations of pinning stones. Figure 42 shows the automatically detected locations of pinning stones for the selected wall section. While visually striking, it must be noted that these results may over-estimate the amount of pinning, due to various approximations used in our current algorithm and its imperfect results. Further improvements of the segmentation algorithm shall improve the pinning estimations.

Beside the estimation of the amount of pinning potentially needed, it is interesting to note that the detection of large non-recessed mortar areas between stones could also be employed to indicate whether cement is likely to have been used in the mortar.

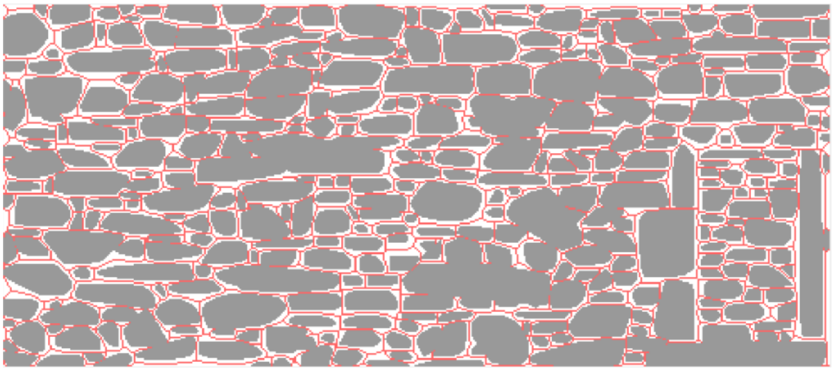

(a) The centre lines of the mortar areas are shown in red.

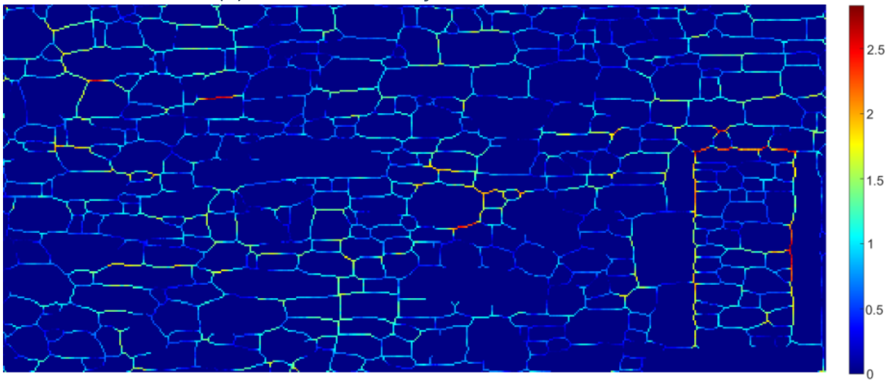

(b) The depth of mortar recess along the mortar centre lines (in centimetres).

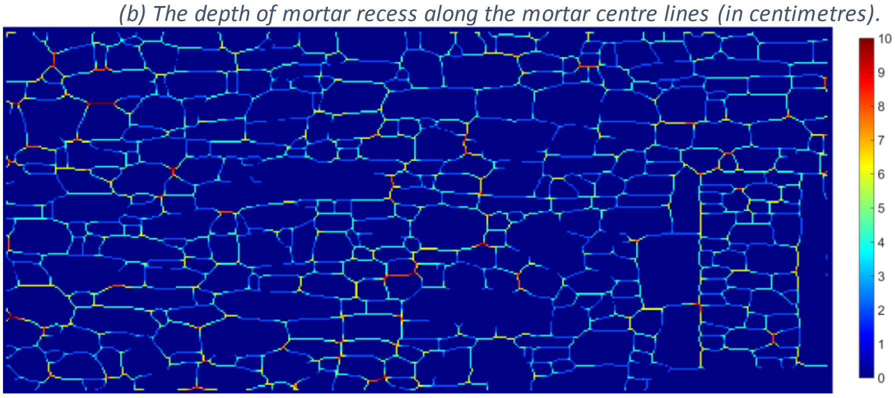

(c) The width of mortar recess along the mortar centre lines (in centimetres).

Figure 41: Automatic measurement of the length (a), depth (b) and width (c) of mortar joints in the selected wall section.

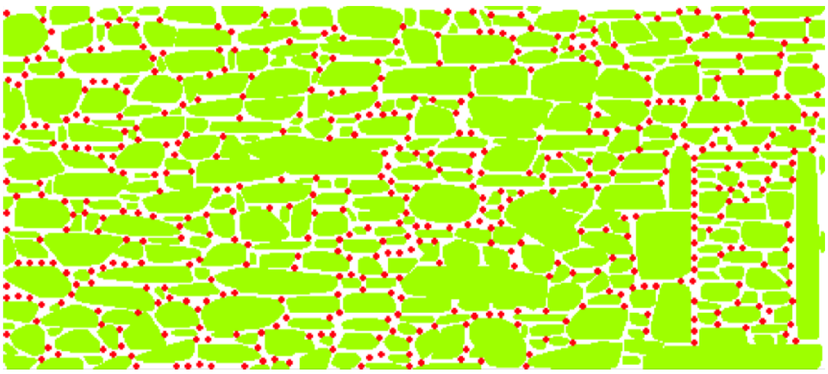

Figure 42: Automated detection of potential pinning stone locations. The stones are shown in green, the mortar regions in white, and the pinning stone location in red.

5 Conclusions

The summarised research in this report provides interesting comparative information for the use of various 3D reality capture technologies for masonry survey. It also demonstrates how novel data processing approaches could support surveyors in extracting valuable information for interpreting the vast quantity of data provided by those survey technologies and extracting information of value to their activities.

Regarding the comparison of the different 3D reality capture technologies, the following conclusions were reached:

- Accuracy:
    - High-end TLS, like the recently released Leica ScanStation P40, provided data with the best accuracy.
    - The cheaper and more portable Faro Focus 3D performed very well, producing data that seemed only slightly less accurate than that of the Leica TLS.
    - The pole-mounted Nikon camera PG system performed remarkably well, with data accuracy almost in par with that of the Faro Focus 3D.
    - In contrast, the UAV system performed poorly. However, the authors have identified that this may have been the result of (unfortunate) decisions regarding the planning of the survey, with the selection of a lens' focal length and an image density that were not compatible to deliver accurate and complete data.
    - In light of this, the authors would recommend conducting a new experiment comparing the pole-mounted and UAV-mounted systems (with P40 as a benchmark) using the exact same camera systems. It is also advised to develop a robust *Planning for Photogrammetry (P4P)* method that defines the picture distance, focal length, camera resolution, camera locations, and other important factors that would altogether ensure that the acquired data deliver 3D reconstructions with sufficient accuracy.
- Completeness
    - TLS (ground-based) performed well for the types of walls surveyed only for walls that do not exceed approximately 8m. Higher, occlusion of the stones on the mortar joints result in incomplete data with small holes in the data.
    - In contrast, the pole-mounted PG system, with a pole climbing only up to 5m was able to completely scan walls up to 10m, but the authors believe that this performance may not be achieved for walls higher than 10m.
    - Mounting the camera system on a UAV alleviates this problem entirely, as long as the UAV can be safely flown in the environment.
- Efficiency:
    - In terms of data acquisition, all systems were fast (we were able to conduct all data acquisition within a day).

    - Data acquisition using the pole-mounted system was nonetheless clearly the fastest, which adds to the value of such systems in practice (that are much cheaper and portable than TLS devices).
    - Data acquisition using the UAV was slower. This was due to the fact that many more pictures had to be taken due to the larger focal length used, and that the UAV batteries had to be changed every 10 minutes, a process that itself took at least 5 minutes. Naturally, it is expected that the autonomy of UAVs will continue increase rapidly as battery technologies develop.
- Stereo-Camera Photogrammetry:
    - Regrettably, the system tested in this project used industrial cameras that performed poorly in the outdoor context of the castle. This made it impossible for the Heriot-Watt team to demonstrate any advantage of using a stereo-camera PG system over a single-camera PG system.
    - It is nonetheless recommended that stereo-image PG be further investigated with the deployment of a more adequate system.

This report highlights the fact that the rapid improvement in 3D reality capture technologies is reducing the time restriction associated with the acquisition stage, which only revealed the next restriction associated with the data processing stage. Within the context of masonry wall survey, such processing would for example enable the evaluation of movement of the wall as an entire element or specific individual stones, recessed mortar joints requiring re pointing, etc. Traditionally, little research has been reported on the development of algorithms that can support surveyors in the processing of the vast amount, of data associated with particularly complex tasks such as surveying random rubble masonry where the stones are all variable in size and shape, do not follow uniform coursing and bonding, and the walls themselves are not necessarily planar. The unique results established in this report (second part of the research) demonstrate that algorithms can be developed that can contribute in easing the data processing restrictions. These results remain preliminary and further studies should be conducted. For example, it would be of interest to assess whether TLS or PG, along with well-crafted algorithms, could deliver accurate geometries of dimensional stones as required in cutting schedules.

References

[1] Health and Safety Executive. (2015) Health and Safety in Construction in Great Britain, 2014. [Online]. Available: http://www.hse.gov.uk/statistics/industry/construction/

[2] A. Straub, "Dutch Standard for Condition Assessment of Buildings," *Structural Survey*, vol. 27, no. 1, pp. 23–35, 2009. [Online]. Available: http://dx.doi.org/10.1108/02630800910941665

[3] A. M. Forster and J. Douglas, "Condition Survey Objectivity and Philosophy Driven Masonry Repair: An Increased Probability for Project Divergence?" *Structural Survey*, vol. 28, no. 5, pp. 384–407, 2010. [Online]. Available: http://dx.doi.org/10.1108/02630801011089173

[4] C. L. Ogleby, "Advances in the Digital Recording of Cultural Monuments," *ISPRS Journal of Photogrammetry and Remote Sensing*, vol. 50, no. 3, pp. 8 – 19, 1995. [Online]. Available: http://dx.doi.org/10.1016/0924-2716(95)91286-S

[5] L. Wilson, A. Rawlinson, D. Mitchell, H. McGregor, and R. Parsons, "The Scottish Ten Project: Collaborative Heritage Documentation," in *International Archives of the Photogrammetry, Remote Sensing and Spatial Information Sciences, Volume XL-5/W2. XIV International CIPA Symposium*, Strasbourg, September 2013.

[6] A. Cardaci, G. M. Roberti, and A. Versaci, "From the Continuous to the Discrete Model: a Laser Scanning Application to Conservation Projects," in *Proceedings of the Congress of the International Society for Photogrammetry and Remote Sensing (ISPRS)*, 2011, pp. 437–444.

[7] A. Nettley, K. Anderson, C. DeSilvey, and C. Caseldine, "Using Terrestrial Laser Scanning and LIDAR Data for Photo-Realistic Visualization of Climate Impacts at Heritage Sites," in *Proceedings of the International Symposium on Photogrammetry, Remote Sensing and Spatial Information Sciences*, 2013, pp. 223–229.

[8] T. Temizer, G. Nemli, E. Ekizce, A. Ekizce, S. Demir, B.Bayram, A. F.H, A. V. Cobanoglu, and H. F. Yilmaz, "3D Documentation of a Historic Monument Using Terrestrial Laser Scanning Case Study: Byzantine Water Cistern, Istanbul," in *International Archives of the Photogrammetry, Remote Sensing and Spatial Information Sciences, Volume XL-5/W2, 2013 XXIV International CIPA Symposium*, Strasbourg, France, 2013, pp. 623–628.

[9] J. D. Matías, F. Berenguer, J. Cortés, J. D. Sanjosé, and A. Atkinson, "Laser Scanning for the Geometric Study of the Alcántara Bridge and Coria Cathedral," in *Proceedings of 3D-ARCH 2013 - 3D Virtual Reconstruction and Visualization of Complex Architectures*, Trento, Italy, 2013, pp. 51–56.

[10] D. Lowe, "Object Recognition from Local Scale-Invariant Features," in *Proceedings of the International Conference on Computer Vision*, vol. 2, 1999, pp. 1150–1157.

[11] H. Bay, T. Tuytelaars, and L. van Gool, "SURF: Speeded Up Robust Features," in *Proceedings of the European Conference on Computer Vision*, 2006.

[12] C. Strecha, T. Tuytelaars, and L. van Gool, "Dense Matching of Multiple Wide-baseline Views," in *Proceedings of International Conference on Computer Vision, ICCV 2003*, Nice, France, 2003.

[13] V. Cappellini, C. Stefani, N. Nony, and L. De Luca, "Surveying Masonry Structures by Semantically Enriched 2.5D Textures: A New Approach," in *Progress in Cultural Heritage Preservation*, ser. Lecture Notes in Computer Science, Springer Berlin Heidelberg, 2012, vol. 7616, pp. 729–737. [Online]. Available: http://dx.doi.org/10.1007/978-3-642-34234-9_77

[14] I. Brilakis, H. Fathi, and A. Rashidi, "Progressive 3D Reconstruction of Infrastructure with Videogrammetry," *Automation in Construction*, vol. 20, pp. 884–895, 2011. [Online]. Available: http://dx.doi.org/10.1016/j.autcon.2011.03.005

[15] F. Bruno, G. Bianco, M. Muzzupappa, S. Barone, and A. Razionale, "Experimentation of Structured Light and Stereo Vision for Underwater 3D Reconstruction," *ISPRS Journal of*

Photogrammetry and Remote Sensing, vol. 66, no. 4, pp. 508 – 518, 2011. [Online]. Available: http://dx.doi.org/10.1016/j.isprsjprs.2011.02.009
[16] D. Turner, A. Lucieer, and C. Watson, "An Automated Technique for Generating Georectified Mosaics from Ultra-High Resolution Unmanned Aerial Vehicle (UAV) Imagery, Based on Structure from Motion (SfM) Point Clouds," *Remote Sensing*, vol. 4, pp. 1392–1410, 2012. [Online]. Available: http://dx.doi.org/10.3390/rs4051392
[17] P. Zarco-Tejada, R. Diaz-Varela, V. Angileri, and P. Loudjani, "Tree Height Quantification Using Very High Resolution Imagery Acquired from an Unmanned Aerial Vehicle (UAV) and Automatic 3D Photo-Reconstruction Methods," *European Journal of Agronomy*, vol. 55, pp. 89–99, 2014. [Online]. Available: http://dx.doi.org/2014. 10.1016/j.eja.2014.01.004
[18] N. Metni and T. Hamel, "A UAV for Bridge Inspection: Visual Servoing Control Law with Orientation Limits," *Automation in Construction*, vol. 17, pp. 3–10, 2007. [Online]. Available: http://dx.doi.org/10.1016/j.autcon.2006.12.010
[19] P. Rodriguez-Gonzalvez, D. Gonzalez-Aguilera, G. Lopez-Jimenez, and I. Picon-Cabrera, "Image-Based Modeling of Built Environment from an Unmanned Aerial System," *Automation in Construction*, vol. 48, pp. 44–52, 2014. [Online]. Available: http://dx.doi.org/10.1016/j.autcon.2014.08.010
[20] H. Püschel, M. Sauerbier, and H. Eisenbeiss, "A 3D Model of Castle Landenberg (CH) from Combined Photogrammetric Processing of Terrestrial and UAV-Based Images," in *The International Archives of the Photogrammetry, Remote Sensing and Spatial Information Sciences*, vol. XXXVII, Beijing, 2008, pp. 93–98.
[21] F. Remondino, L. Barazzetti, F. Nex, M. Scaioni, and D. Sarazzi, "UAV Photogrammetry for Mapping and 3D Modeling - Current Status and Future Perspectives," in *International Archives of the Photogrammetry, Remote Sensing and Spatial Information Sciences*, vol. XXXVIII-1/C22, 2011, pp. 25–31.
[22] F. Remondino, "Heritage Recording and 3D Modeling with Photogrammetry and 3D Scanning," *Remote Sensing*, vol. 3, pp. 1104–1138, 2011. [Online]. Available: http://dx.doi.org/10.3390/rs3061104
[23] A. Koutsoudis, B. Vidmar, G. Ioannakis, F. Arnaoutoglou, G. Pavlidis, and C. Chamzas, "Multi-Image 3D Reconstruction Data Evaluation," *Journal of Cultural Heritage*, vol. 15, pp. 73–79, 2014. [Online]. Available: http://dx.doi.org/10.1016/j.culher.2012.12.003
[24] Z. Xu, L. Wu, Y. Shen, F. Li, Q. Wang, and R. Wang, "Tridimensional Reconstruction Applied to Cultural Heritage with the Use of Camera-Equipped UAV and Terrestrial Laser Scanner," *Remote Sensing*, vol. 6, pp. 10413–10434, 2014. [Online]. Available: http://dx.doi.org/10.3390/rs61110413
[25] Y. Arayici, "Towards Building Information Modelling for Existing Structures," *Structural Survey*, vol. 26, no. 3, pp. 210–222, 2008. [Online]. Available: http://dx.doi.org/10.1108/02630800810887108
[26] D. Andrews, J. Bedford, and P. Bryan, "A Comparison of Laser Scanning and Structure for Motion as Applied to the Great Barn at Harmondsworth, UK," in *International Archives of the Photogrammetry, Remote Sensing and Spatial Information Sciences, Volume XL-5/W2, 2013 XXIV International CIPA Symposium*, Strasbourg, France, 2013, pp. 31–36.
[27] H. Macher, T. Landes, P. Grussenmeyer, and E. Alby, "Semi-automatic Segmentation and Modelling from Point Clouds towards Historical Building Information Modelling," in *Digital Heritage. Progress in Cultural Heritage: Documentation, Preservation, and Protection*, ser. Lecture Notes in Computer Science, Springer International Publishing, 2014, vol. 8740, pp. 111–120. [Online]. Available: http://dx.doi.org/10.1007/978-3-319-13695-0_11
[28] J. Meneely, B. Smith, J. Curran, and A. Ruffell, "Developing a Non-Destructive Scientific Toolkit to Monitor Monuments and Sites," in *Proceedings of ICOMOS Scientific Symposium*, 2009.
[29] N. Hichri, C. Stefani, L. D. Luca, P. Veron, and G. Hamon, "From Point Cloud to BIM: A Survey of Existing Approaches," in *International Archives of the Photogrammetry, Remote Sensing and*

Spatial Information Sciences, Volume XL-5/W2, 2013 XXIV International CIPA Symposium, Strasbourg, France, 2013, pp. 343–348.

[30] D. Oreni, R. Brumana, F. Banfi, L. Bertola, L. Barazzetti, B. Cuca, M. Previtali, and F. Roncoroni, "Beyond Crude 3D Models: From Point Clouds to Historical Building Information Modeling via NURBS," in *Digital Heritage. Progress in Cultural Heritage: Documentation, Preservation, and Protection*, ser. Lecture Notes in Computer Science, Springer International Publishing, 2014, vol. 8740, pp. 166–175. [Online]. Available: http://dx.doi.org/10.1007/978-3-319-13695-0_16

[31] S. Garagnani and A. M. Manferdini, "Parametric Accuracy: Building Information Modeling Processs Applied to the Cultural Heritage Preservation," in *Proceedings of 3D-ARCH 2013 - 3D Virtual Reconstruction and Visualization of Complex Architectures*, Trento, Italy, 2013, pp. 87–92.

[32] M. L. V. Baptista, "Documenting a Complex Modern Heritage Building Using Multi Image Close Range Photogrammetry and 3D Laser Scanned Point Clouds," in *International Archives of the Photogrammetry, Remote Sensing and Spatial Information Sciences, Volume XL-5/W2, 2013 XXIV International CIPA Symposium*, Strasbourg, France, 2013, pp. 675–678.

[33] X. Brunetaud, L. D. Luca, S. Janvier-Badosa, K. Beck, and M. Al-Mukhtar, "Application of Digital Techniques in Monument Preservation," *European Journal of Environmental and Civil Engineering*, vol. 16, no. 5, pp. 543–556, 2012. [Online]. Available: http://dx.doi.org/10.1080/19648189.2012.676365

[34] T. Cardinale, R. Valva, and M. Lucarelli, "The Integrated Survey for Excavated Architectures: the Complex of Casalnuovo District with the World Heritage Site "Sassi" (Matera, Italy)," in *Proceedings of 3D Virtual Reconstruction and Visualization of Complex Architectures*, 2015, pp. 403–409.

[35] ICOMOS, *ICOMOS-ISCS: Illustrated Glossary on Stone Deterioration Patterns*, ICOMOS, 2008.

[36] L. Moltedo, G. Mortelliti, O. Salvetti, and D. Vitulano, "Computer Aided Analysis of the Buildings," *Journal of Cultural Heritage*, vol. 1, pp. 59–67, 2000. [Online]. Available: http://dx.doi.org/10.1016/S1296-2074(99)00115-6

[37] R. Cossu and L. Chiappini, "A Color Image Segmentation Method as Used in the Study of Ancient Monument Decay," *Journal of Cultural Heritage*, vol. 5, pp. 385–391, 2004. [Online]. Available: http://dx.doi.org/10.1016/j.culher.2004.03.005

[38] M. J. Thornbush and H. Viles, "Photographic Monitoring of Soiling and Decay of Roadside Walls in Central Oxford, England," *Environmental Geology*, vol. 56, no. 3-4, pp. 777–787, 2008. [Online]. Available: http://dx.doi.org/10.1007/s00254-008-1311-3

[39] P. Kapsalas, M. Zervakis, and P. Maravelaki-Kalaitzaki, "Evaluation of Image Segmentation Approaches for Non-Destructive Detection and Quantification of Corrosion Damage on Stonework," *Corrosion Science*, vol. 49, pp. 4415–4442, 2007. [Online]. Available: http://dx.doi.org/10.1016/j.corsci.2007.03.049

[40] M. M. Cerimele and R. Cossu, "Decay Regions Segmentation from Color Images of Ancient Monuments Using Fast Marching Method," *Journal of Cultural Heritage*, vol. 8, pp. 170–175, 2007. [Online]. Available: http://dx.doi.org/10.1016/j.culher.2007.01.006

[41] M. M. Cerimele and R. Cossu, "A Numerical Modelling for the Extraction of Decay Regions from Color Images of Monuments," *Mathematics and Computers in Simulation*, vol. 79, pp. 2334–2344, 2009. [Online]. Available: http://dx.doi.org/10.1016/j.matcom.2009.01.015

[42] N. Oses and F. Dornaika, "Image-Based Delineation of Built Heritage Masonry for Automatic Classification," in *Image Analysis and Recognition*, ser. Lecture Notes in Computer Science, M. Kamel and A. Campilho, Eds. Springer Berlin Heidelberg, 2013, vol. 7950, pp. 782–789. [Online]. Available: http://dx.doi.org/10.1007/978-3-642-39094-4_90

[43] E. Angelopoulu and J. R. Wright, "Laser Scanning Technology," University of Pennsylvania, Tech. Rep., 1999.

[44] D. Huttenlocher, G. Klanderman, and W. Rucklidge, “Comparing Images Using the Hausdorff Distance,” *IEEE Transactions on Pattern Analysis and Machine Intelligence*, vol. 15, no. 9, pp. 850–863, 1993. [Online]. Available: http://dx.doi.org/10.1109/34.232073
[45] M. Kazhdan, M. Bolitho, and H. Hoppe, “Poisson Surface Reconstruction,” in *Eurographics Symposium on Geometry Processing*, 2006.
[46] CRC Press, *Spon’s Architects and builders price book*. CRC Press, 2014.
[47] Franklin & Andrews, *Griffiths Complete Building Price Book*. Franklin & Andrews, 2015.
[48] RICS, *RICS New Rules of Measurement - NRM 2: Detailed Measurement for Building Works*. RICS Books, 2012.